

# Impact of High-Resolution Variational Assimilation on Short-Range QPF over Gard area

GMAP

GROUPE DE MODÉLISATION POUR L'ASSIMILATION ET LA PRÉVISION

CENTRE NATIONAL DE  
RECHERCHES MÉTÉOROLOGIQUES

MÉTÉO-FRANCE

ANDREA STORTO

TOULOUSE, MARCH-SEPTEMBER 2005

# Contents

<b>Résumé Abstract Riassunto</b>	<b>ii</b>
<b>1 Introduction</b>	<b>1</b>
<b>2 The experiments</b>	<b>4</b>
2.1 The Case of study . . . . .	4
2.2 Observations . . . . .	5
2.3 Definition of the experiments and practical implementation . . . . .	7
2.4 Models configuration . . . . .	9
<b>3 Results</b>	<b>10</b>
3.1 Structure of analyzed fields . . . . .	10
3.2 Radiosonde comparison . . . . .	16
3.3 Subjective verification of rainfall . . . . .	19
3.4 Verification of surface quantities by scores comparison . . . . .	26
3.5 Verification of QPFs by scores comparison . . . . .	26
<b>4 Conclusions</b>	<b>34</b>
<b>A Assimilation of 2m temperature for cycling experiment</b>	<b>35</b>
<b>B The error background covariances used in the simulations</b>	<b>38</b>
<b>C Test with assimilation of MSG/SEVIRI radiances</b>	<b>40</b>
<b>References</b>	<b>43</b>

# Résumé

De nos jours l'assimilation variationnelle représente la procédure la plus utilisée pour effectuer l'analyse des conditions initiales au sein des modèles atmosphériques. D'autre part, les modèles mésoéchelle opérationnels ne permettent pas de résoudre explicitement les phénomènes de convection (2.5 km). Afin que la résolution de l'analyse soit cohérente avec le modèle prévisionnel et que les données asynoptiques (satellites, radars, etc.) puissent être mieux exploitées, notamment si les objectifs sont la prévision à court terme (jusqu'à 12 heures) et la prévision de pluies intenses, nous utilisons une méthode d'assimilation fondée sur deux analyses indépendantes 3D-Var respectivement de 10 et 2.5 km de résolution. Le modèle de prévision (Mésos-NH) combine ces 2 analyses. Il apparaît que cette méthode d'assimilation permet d'obtenir des résultats plus proches des valeurs observées qu'avec les analyses traditionnelles. Au travers de cette analyse nous avons aussi pu mettre en évidence l'impact positif des observations à 2 mètres.

# Abstract

Nowadays variational assimilation represents the most popular procedure to achieve analysis of initial conditions in atmospheric modeling. Operational mesoscale models are reaching up the convection-resolving scale (2.5km). In order to keep coherency between resolution of assimilation model and forecasting model, and to better profit by the potential of asynoptic data (satellites, radar, etc.), specially when the aim is short-range forecasts (up to 12 hours) and precipitation forecasts, the impact of an assimilation based on two independent 3D-Var analysis at resolution of 10 and 2.5 km is presented. Forecasting model (Mésos-NH) uses both of them by interactive nesting. Such a method allows to analysis and forecasts to be closer to observations rather than with traditional resolution. Results focus also on the benefits of 2-meters observations.

# Riassunto

L'assimilazione variazionale rappresenta oggi la tecnica più largamente

utilizzata per ottenere l'analisi delle condizioni iniziali nei modelli atmosferici. Nello stesso tempo un grande sforzo è compiuto per portare i modelli a mesoscala a una risoluzione che possa risolvere esplicitamente i fenomeni convettivi (2.5 km). La risoluzione dei modelli di assimilazione deve risultare coerente con quella del modello previsionale, essendo inoltre tale risoluzione in grado di sfruttare meglio le potenzialità delle osservazioni asinottiche (satellite, radar, etc.), specialmente quando l'obiettivo sono le previsioni a corto termine (fino a 12 ore) e interessano gli eventi di pioggia intensa. Viene qui presentato l'impatto di un'assimilazione consistente in due analisi 3D-Var indipendenti alla risoluzione di 10 e 2.5 km rispettivamente, sfruttate entrambe dal modello di previsione (Mésos-NH) attraverso l'integrazione su due griglie innestate. Tale metodo produce dei risultati più vicini alle osservazioni rispetto all'assimilazione alla scala tradizionale. Attenzione si è inoltre posta sul positivo impatto delle osservazioni a 2 metri.

# 1 Introduction

The correct forecast of rainfall is an important issue connected with civil protection. In fact, strong precipitation might cause increase in rivers flow, up to overflow, and urban drainage. In such cases the advanced knowledge of both storm localization and intensity could save lives and limit economical damages (mainly in the domain of agriculture). The increase of resolution in forecasting models represents of course a way to improve precipitation forecasts especially for short-range forecasting (on which such an approach is addressed by nature for the short-range predictability of convective systems), at least when data dissemination allows it (Ducrocq et al., 2002), since if the resolution arrives to about 2.5 km convection is no more a subgrid phenomenon. With computer evolution, such a framework can be competitive with traditional nowcasting tools based on images analysis, and it can succeed to become operational.

Furthermore, because this resolution plays role of subgrid parametrization itself, adding a two-way interactive grid-nesting method to model configuration enhances the forecasts on the whole considering that even the large-scale model profits by it (Stein et al., 2000). Convection-resolving scale gets bigger consistency with asynoptic observing system (geostationary satellites, meteo-radars), whose importance in short-range precipitation forecasts is basic because of the lack of information about the vertical structure of humidity fields by the use of conventional observations. In particular, one can expect that the success of mesoscale high-resolution models in forecasting short-range precipitations, in comparison with nowcasting approaches, could depend on the correct ingestion of radar reflectivity in order to initialize the distribution of hydrometeors, since nowadays explicit variational schemes to do this are yet in a preliminary state (Xiao, 2005), given the strongly non-linear relations between radar observations and model variables. Finally, it shouldn't neglect that such a resolution could turn out to coupled models advantages (for instance hydrological models, fine-scale models for pollutants dispersion and air quality in general, urban meteorology models, nowcasting tools to forecast visibility conditions, etc.). For all these reasons, a lot of National Weather Services and meteorological institutions are addressing their efforts in building an integrated assimilating and forecasting meso-gamma model – see for instance Michalakes et al. (2001) for the WRF project at NCAR and Barker et al. (2004) for what specifically regards his data assimilation system, Bouttier (2003) for the Arome project at Météo-France, Ballard et al. (2005) for the Unified Model project or Steppeler et al. (2003) for the Lokal Modell of COSMO Members.

The main ways to improve precipitation forecasts are to employ more accurate microphysical parameterizations and to enhance the data assimilation. Concer-

ning the second aspect, several procedures of assimilation could be used in order to understand the state of the atmosphere, and all of them are able to improve forecasts instead of a simple interpolation from synoptic analysis (Faccani et al., 2003). Three-dimensional variational assimilation is chosen as analysis procedure in the simulations because:

- Variational assimilation reproduces the state of atmosphere taking into account physical constraints: it can reduce initialization problems (spin-up) in comparison with optimal interpolation systems (Pailleux, 1997) and can recover problems of lack of data (for instance of humidity), mainly for the first 12 hours (Bengtsson and Hodges, 2005);
- It represents the optimal compromise between accuracy of analysis and computational cost (a key-aspect in short-range forecasts), since a mesoscale 4D-Var seems to be yet too expensive, and his benefits regard mainly medium-term forecasts (Gustafsson et al., 1997);
- It has the capability of ingesting in a relatively easier way data retrieved by different networks and instruments.

Anyway, when resolution grow up to the so-called meso-gamma scale, the succeeding extension of 3D-Var analysis becomes not obvious: at this scale geostrophic balance could not result verified and, further, non ad hoc error statistics may compromise all the assimilation cycle. In this context, some researches (Faccani et al., 2003) have pointed out how optimal interpolation is a more efficient method, especially in case of observations abundance.

Another challenge on which investigations are required regards the temporal step of the assimilation cycle, that sometimes has influenced the analysis more than the assimilation method itself (Faccani and Ferretti, 2005). In this sense, further to that one operationally used at Météo-France for his mesoscale model (3D-Var with a 6-hours time-window), several experiments with an hourly assimilation cycle have been run, since such a choice should enhance quantitative precipitation forecasts (Ferretti and Faccani, 2005). In fact, a shorter time-window between assimilation updates could approach the analysis background to the true state of atmosphere; on the other hand spin-up problems are easier to arise (Dance, 2004). Because of difficulties in using 2-meters data in some simulations (with hourly updates), this can be partially seen as a way to evaluate the impact of these observations, even if specific studies should be conducted in this sense to better understand the role of the background covariance errors in a cycling experiment rather than the observations.

The employed methodology uses the interpolated Arpège analysis as backgrounds. The Arpège global model provides also the lateral boundary conditions

(LBC) coupled to the model every 6 hours. The 3D-Var procedure is performed by Aladin-3DVar over two domains at increasing resolution of about 10 and 2.5 km and decreasing extension (hereafter called “Model 1” and “Model 2” respectively, with a little bit perplexing nomenclature). These domains will be the same ones used by the forecasting models with a two-way interactive nesting. This method was successfully applied for short-range forecasts over complex orography domain (Jaubert et al., 2005), but in that case assimilation procedure has consisted of a modified optimal interpolation scheme; so, using 3D-Var has to be tested. Verification of results consists of radiosonde comparison of analysis and forecasts, intercomparison of experiments outputs, scores of 2-meters quantities and QPFs. No comparison with operational forecasts is here supplied. Finally, some experiences have been conducted with mesoscale model Arome instead of Méso-NH. Such simulations had the aim to test the potential of an operational framework<sup>1</sup> inside which Arome could become the forecasting model for the assimilation with hourly update. As experiments with this assimilating configuration have had negative impact on forecasts, Arome forecasts won’t be presented.

---

<sup>1</sup>Because of his dynamical configuration, the computational cost of Arome is much less expensive than Méso-NH; anyway, because of the policy of reducing computational time, it can’t nest two domains simultaneously.

## 2 The experiments

### 2.1 The Case of study

The area focused during the simulations is the Mediterranean Languedoc. In this region flash-floods are not uncommon events (the number of daily precipitations greater than 190 mm arrives to 144 between 1958 and 1994, Jacq (1994)). Main causes can be seen in the key-role of Mediterranean Sea as source of moisture, the orographic characterization of the zone which with its reliefs (Alps, Pyrenees and Massif Central Mountains) encourages convection phenomena when synoptic conditions are destabilizing (Delrieu and al., 2005); heavy rainfall can be caused by both convective and non-convective processes. Evidently such events can represent a human and social danger, as during the flash-flood of 9 September 2002 because of which 24 people died, or more recently during the flash-flood of 5 and 6 September 2005 when in 2 day precipitation exceeded 200 mm causing heavy drainage problems in Montpellier and Nîmes, soil saturation in the basins of Vidourle and Vistre and interrupting railway communication in the interested departments. During this day an active storm line Nord/Sud oriented stations over Gard area.

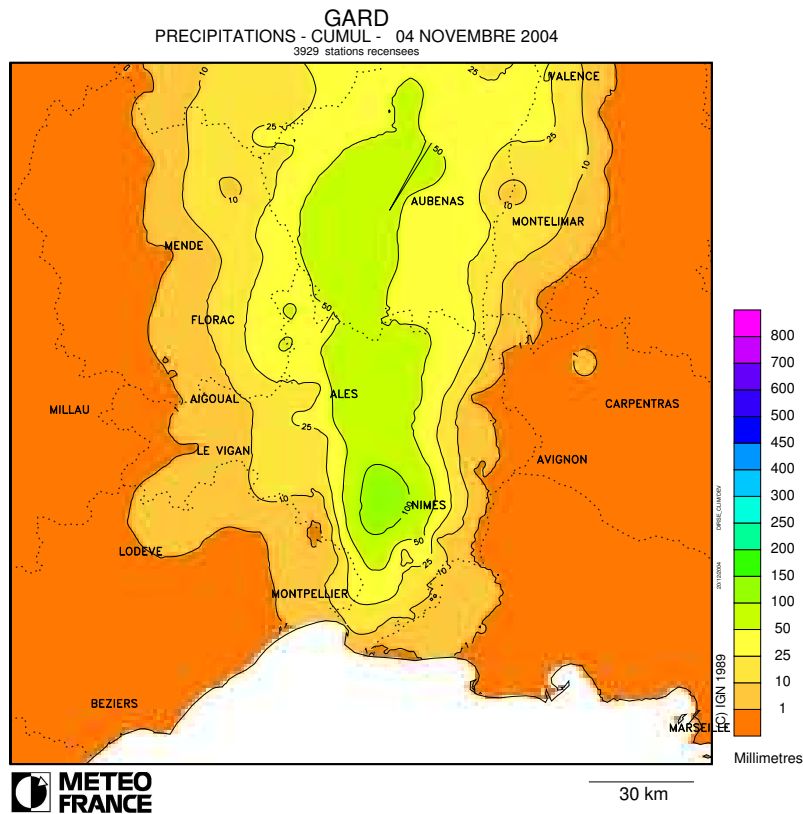
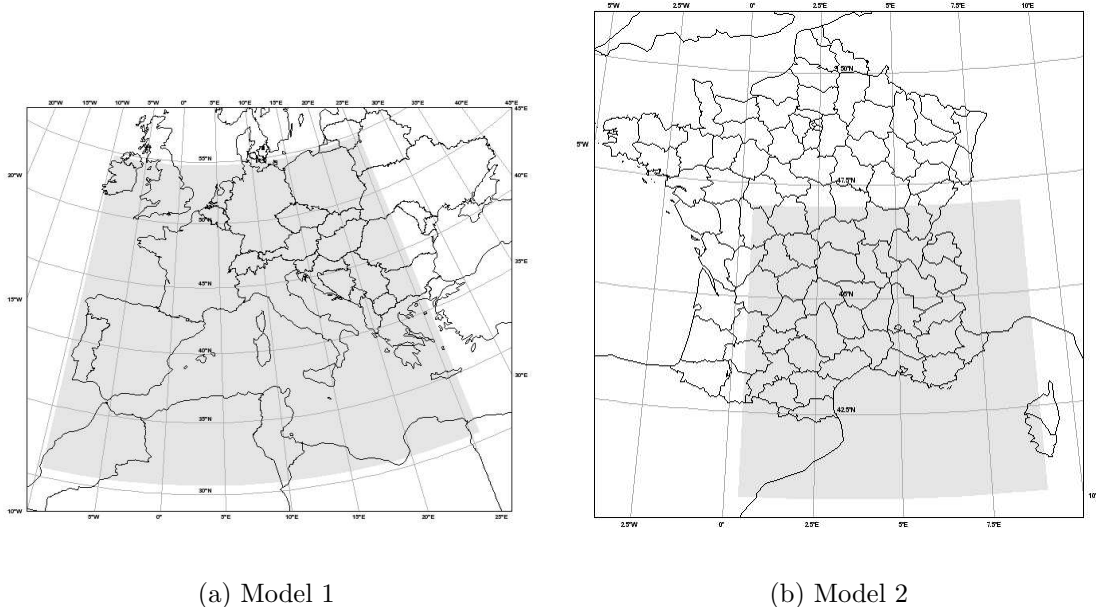


Figure 1: 24-hours cumulated precipitation over Languedoc region on 4 November 2004

The forecasting period is chosen between the 00:00 and 12:00 of 4<sup>th</sup> of November

2004; during these hours precipitations reach up to  $70 \text{ mm} \cdot (12\text{hr})^{-1}$  over Gard area (a maximum of  $146 \text{ mm}$  measured at Nîmes–Mas de Ponge on 4 November, see Fig. 1, with  $19.5 \text{ mm}$  in 15 minutes at about 09 a.m. at Nîmes–Courbessac). The stable profile and the absence of precipitative events at the beginning of simulations should limit initialization problems. The geometry of domain is imposed in order to center Model 1 and Model 2 on the Gard Area; extension and resolution are different. Fig. 2 shows the domain extensions: Model 2 extends from Pyrenees to Alps and from Corse to Massif Central Mountains (Fig. 3 shows the orography of Model 2).



**Figure 2:** Extension of the domains

Synoptic conditions present a low moving eastward close to British Isles, with a secondary low centered on the Mediterranean Sea close to the Tunisian Gulf of Gabes.

## 2.2 Observations

Only conventional observations are set to be active in the analysis. For experiments with hourly assimilation, after some verifications (see App. A), 2 meters observations of temperature and humidity have been excluded; anyway, such these observations are not assimilated in operational Aladin-3DVar. Furthermore, the sensitivity to MSG/SEVIRI radiances has been tested (see App. C). In Tab. 1 the list of data is showed, while in Fig. 5, 6, 7 is presented the dissemination of conventional data, of 2 meters observations and the 10 meters wind measurements respectively. 4 radiosondes at synoptic hours, 5 aircraft reports and 6 balloon measurements are also available between 6 and 12 p.m.. Depending on observation time,

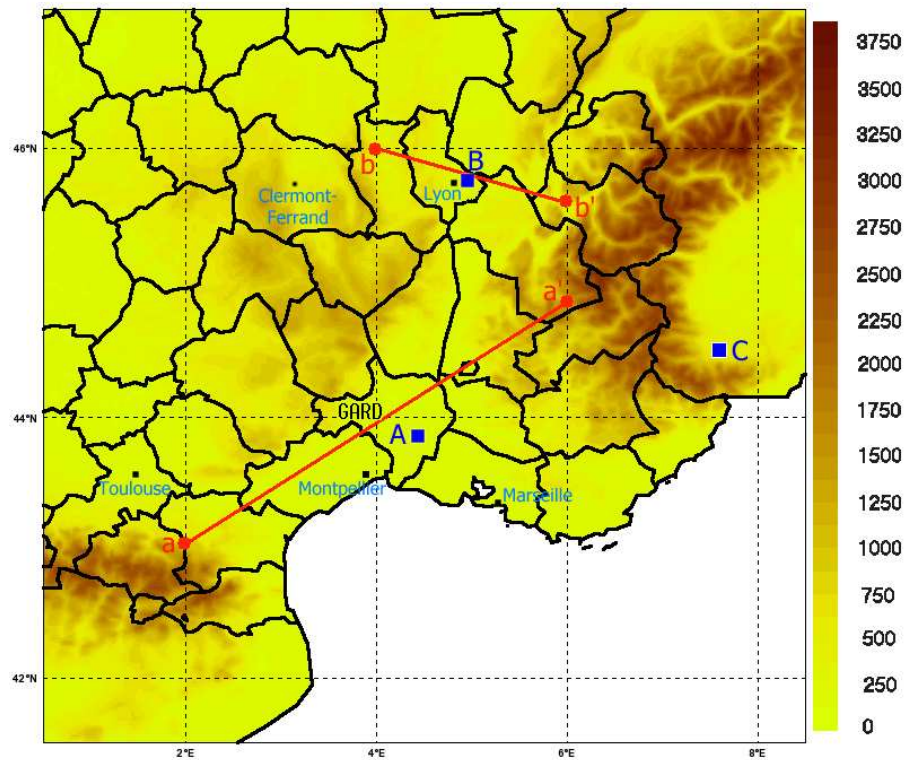
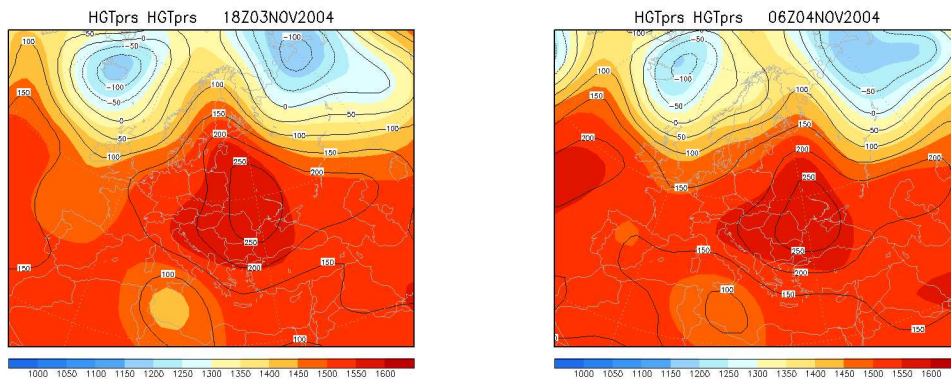


**Figure 3:** Orography of Model 2. Cross-sections and soundings used in Sect. 3 can be seen here.



(a) 3 November - 1800

(b) 4 November - 0600

**Figure 4:** 850 hPa geopotential height (shaded) and 1000 hPa geopotential height (isocontoured) from NOAA reanalysis

measurements of 2m temperature range from a minimum of 396 to a maximum of 588, relative humidity from 326 to 470 and 10 meters wind from 302 to 380. All precedents numbers refer to the domain of Model 2.

Source	A00AA
SYNOP	$U, U_{10}, D, F, H, H_2, T, T_2, Z, P_S, Q$
AIREP	$U, U_{10}, D, F, H, T, Q$
TEMP	$U, U_{10}, D, F, H, T, Q$
DRIBU	$U, U_{10}, Z$
PILOT	$U, U_{10}, D, F$

Table 1: Assimilated observations

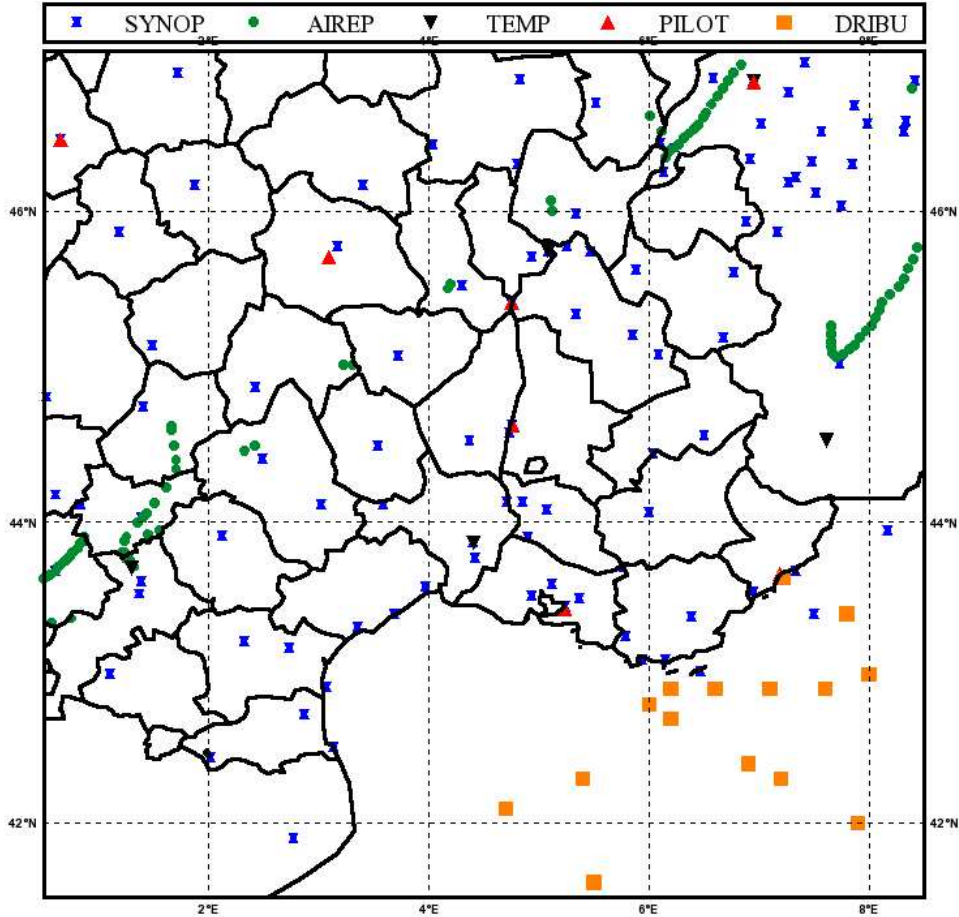
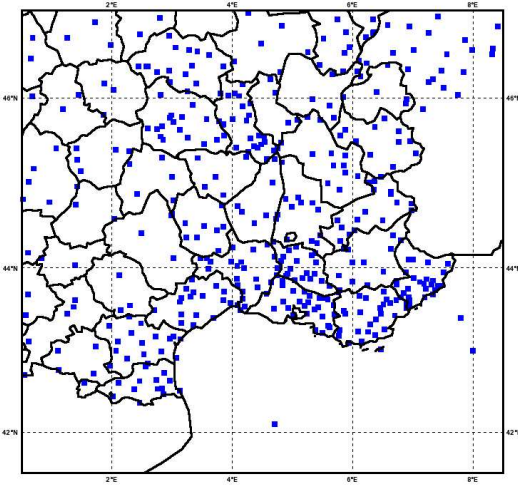


Figure 5: Data dissemination of conventional network

### 2.3 Definition of the experiments and practical implementation

Several experiments have been achieved in order to test the influence of datasets, the background error covariances, the temporal step of assimilation. Two reference experiments are considered in the comparison of assimilation benefits: one starting with Analysis from the Arpège global model without any data assimilation and the other with assimilation only at the resolution of  $10km$ . Tab. 2 shows the



**Figure 6:** Dissemination of temperature and humidity observations at 2 meters a.g.l.

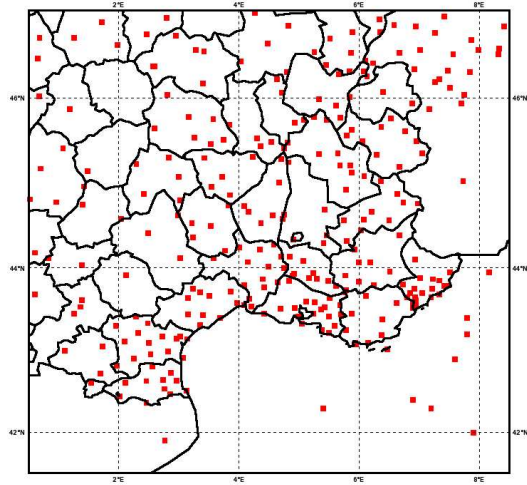


**Figure 7:** Dissemination of wind observations at 10 meters a.g.l.

features of the experiments.

Exp	Assimilation	Strategy	$t$ -window	Observations	$J_B$
<i>RR</i>	–	–	–	–	–
<i>AR</i>	10km	COLD	6hr	STD	A
<i>AA</i>	10km and 2.5km	COLD	6hr	STD	A
AJ	10km and 2.5km	COLD	6hr	STD	B
CD	10km and 2.5km	WARM	1hr	STD	A
CJ	10km and 2.5km	WARM	1hr	STD	B
CA	10km and 2.5km with <i>S.A.</i>	WARM	1hr	STD	B
<i>CC</i>	10km and 2.5km	WARM	1hr	STD without 2m obs	B
SS	10km and 2.5km	COLD	6hr	STD with MSG/SEVIRI	A

**Table 2:** Experiments features. Only the results of those ones whose name is emphaized are presented in Sect. 3. *S.A.* in assimilation of Exp. CA means Surface Analysis, STD set of Observations refers to Tab. 1 and differences between the two  $J_B$  are presented in App. B.

For all the experiments, analysis and not operational forecasts from Arpège supply both the background for 3D-Var and the LBC for Méso-NH. In all the 6 hours cycle experiment 3D-Var is performed using all the observations present in that time-window. For hourly updating assimilations, while the first analysis at 6 p.m. is achieved by using an Arpège background and the hourly observations<sup>2</sup>, for successive analysis the background is provided by an 1-hour integration of Méso-NH of the former analysis. A balance between Model 1 and Model 2 is anyway performed before integration in order to reduce spin-up effects (Faccani and Ferretti, 2005).

<sup>2</sup>The term “warm” which refers to initialization strategy is not rigorous.

## 2.4 Models configuration

The assimilation is performed by the limited area spectral model Aladin (Radnóti et al. (1995) and Široka et al. (2003) for 3D-Var features) with his 3D-Var tool. No black-list is used to reject observations; on the contrary a screening procedure is activated. Reference version of Aladin is cycle 28t2.

The mesoscale forecasting model is the non-hydrostatic anelastic mesoscale model Méso-NH (Lafore et al., 1998). Basic feature of this model is to allow two-way interactive nesting between two grids (Clark, 1984) initialized with independent analysis. The main physical schemes implemented in the simulations are the “ECMWF” scheme for radiation (Morcrette, 1989), the “Kain-Fritsch” (Kain and Fritsch, 1990) scheme for the parametrization of convection in the coarser model (while in the finer one there’s no need of parametrization), the maximum verbosity level for hydrometeors (Pinty and Jabouille, 1999), the one and half order closure for turbulent kinetic energy equation (Cuxart et al., 2000) – mono-dimensional for Model 1 and three-dimensional for Model 2 – and the “ISBA” scheme (Boone et al., 1999) for parametrization of superficial fluxes. In both Model 1 and Model 2 the number of grid-point is set to  $288^3$  and the center is at longitude  $4.5^\circ\text{E}$  and latitude  $44.0^\circ$ . Vertical levels are 41, vertical resolution is the same in Aladin and Méso-NH, it decreases with height being stretched from a minimum spacing of 72 m at ground level (hereafter the first model level above ground will be called  $T_{41}$ , and so on decreasing for the other ones) to a maximum, for the last two levels at 20 km of height, of 1024 m.

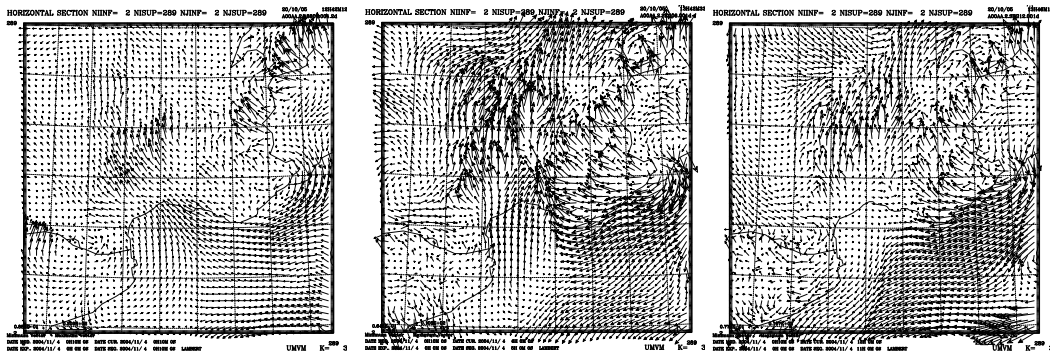
---

<sup>3</sup>300 in Aladin-3DVar since the extension-area is increased to include boundary effects in the spectral space.

### 3 Results

#### 3.1 Structure of analyzed fields

Mesoscale circulation in the area is characterized by the orographic forcing. The Gulf of Marseille and the large valley in the northern part of domain play main role representing a corridor for the flows coming from the sea. Such winds grow up in the early hours of the morning because of the contribution of sea-breezes and mountain flows from Alps, tending later to move clockwise. These elements recur in every simulation, but appear amplified in all but the *AA*.

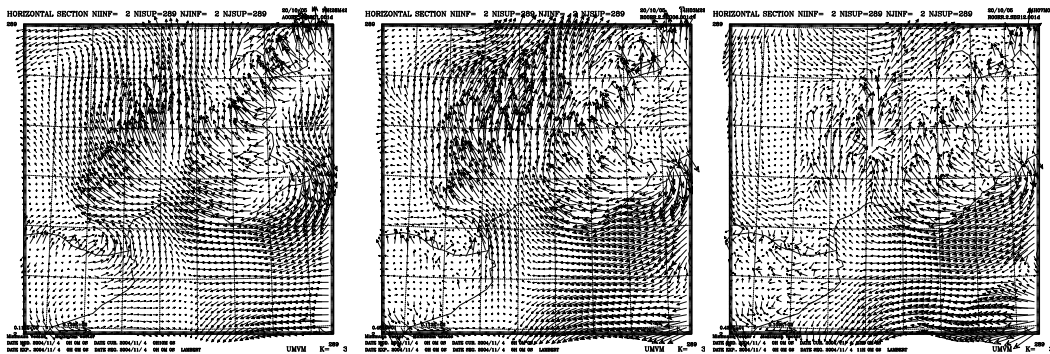


(a) AT

(b) AT + 6hr

(c) AT + 12hr

**Figure 8:** Exp. *AA* - Horizontal wind at 72 m a.g.l.



(a) AT

(b) AT + 6hr

(c) AT + 12hr

**Figure 9:** Exp. *RR* - Horizontal wind at 72 m a.g.l.

In the area where precipitation will be produced later, Exp. *AA* shows different analysis for both temperature and humidity. This generic behavior is damped in the following forecasted hours but it's enough to justify the different rain rates

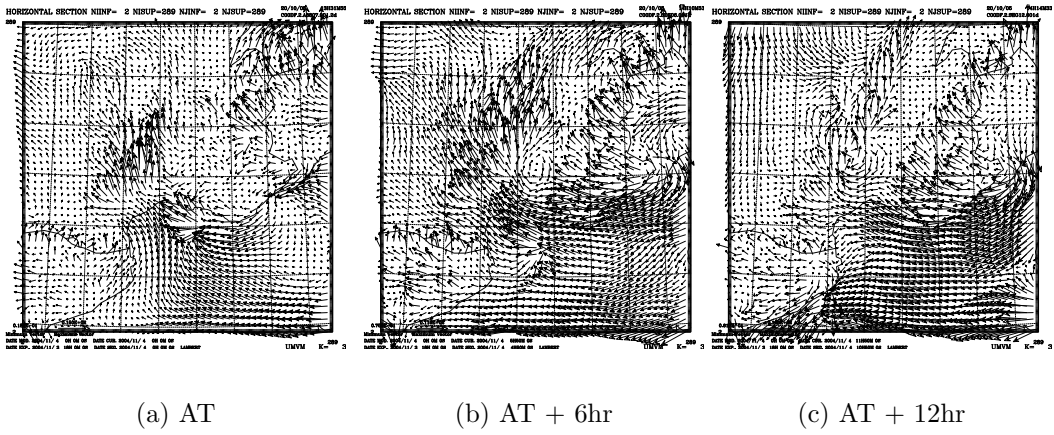


**Figure 10:** Exp. *CC* - Horizontal wind at 72 m a.g.l.

produced. Examining two sections (see Fig. 3) that cross the storm line<sup>4</sup>, potential temperature profile is characterized by reaching up to lower values at levels close to ground in respect of other experiments, including *CC*; in other words profile at low atmosphere presents a more marked stable behavior for Exp. *AA* at analysis time (midnight).

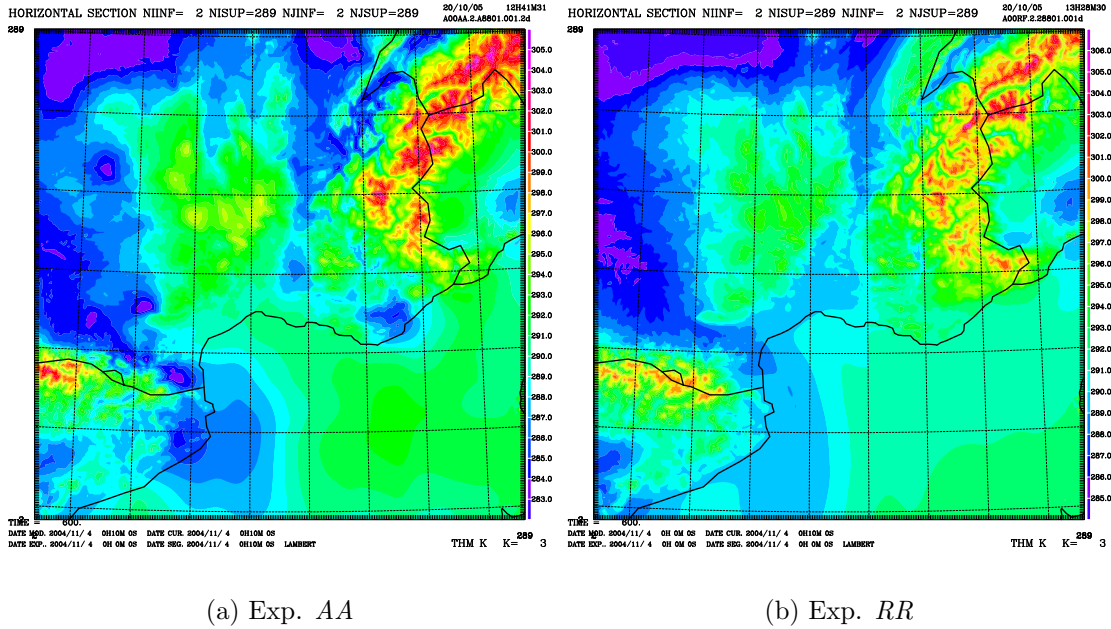


**Figure 11:** Potential temperature at 72 m a.g.l.. Experiments *AR* and *CC* present a very similar field of *RR*

This is not true in general for the overall domain of Model 2, but it appears

<sup>4</sup>The cross-section *a-a'* extends from (2.00°E;43.00°N) to (6.00°E;44.86°N) for a length of 381.3km, while cross-section *b-b'* from (4.00°E;46.00°N) to (6.00°E;45.54°N) for 163.4km. Both of them reach a radiosonde station, A and B respectively.

evident over the Gard area (see Fig. 11). For the same cross-sections, profiles of humidity are presented. Main anomalies could be seen in low-levels field, where humidity difference exceeds 20%, in particular in the eastern part of domain. Experiments *RR* and *CC* tend to underestimate humidity, up to neglect convection arising especially over the valleys close to Alps. More difficult is evaluation of comparison of vertical wind profiles, not showed.

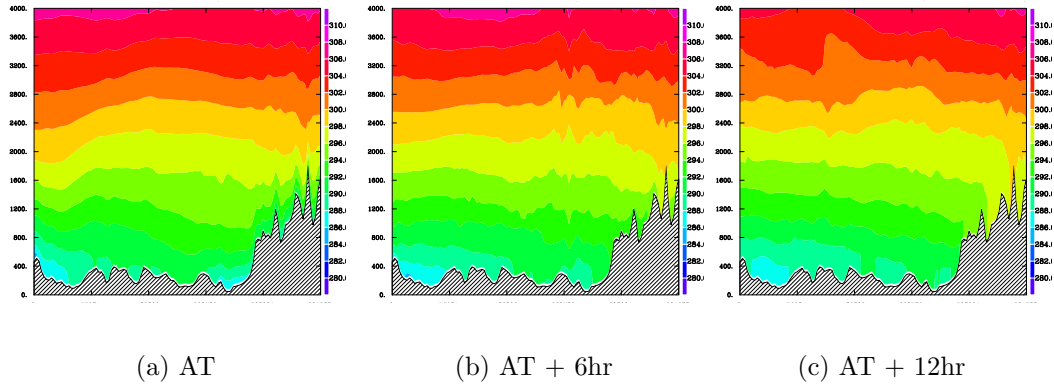


**Figure 12:** Exp. *AA* - Potential temperature for a-a'

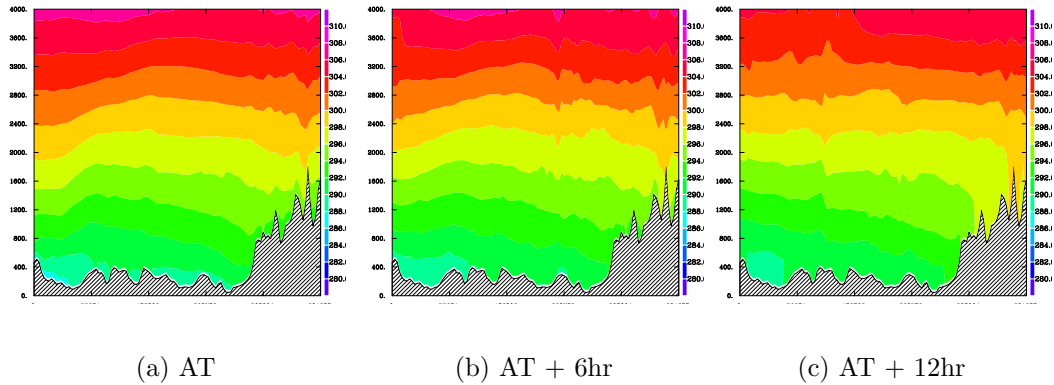


**Figure 13:** Exp. *RR* - Potential temperature for a-a'

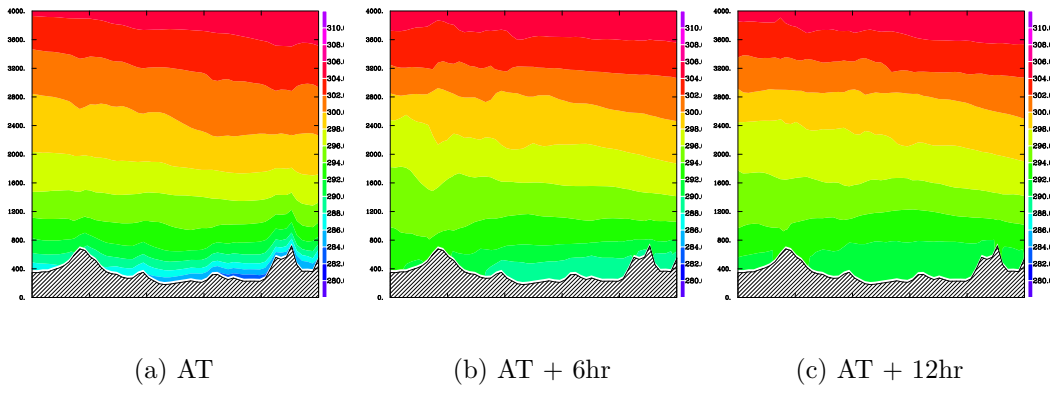


**Figure 14:** Exp. *AA* - Potential temperature for b-b'

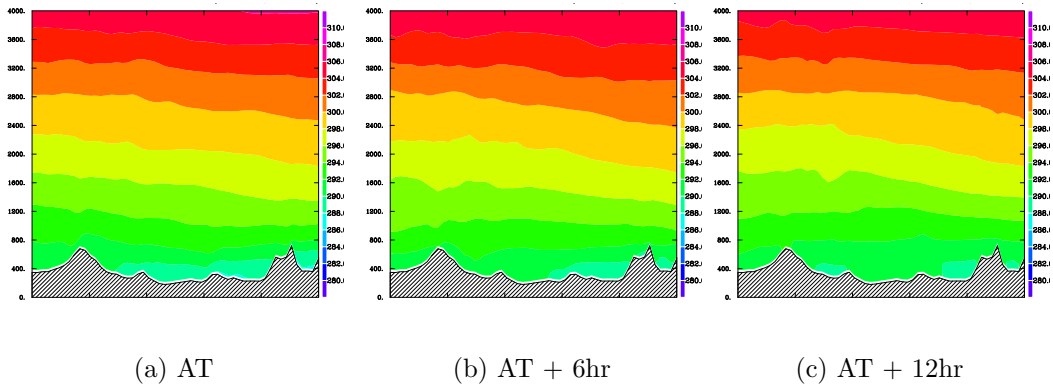


**Figure 15:** Exp. *CC* - Potential temperature for b-b'

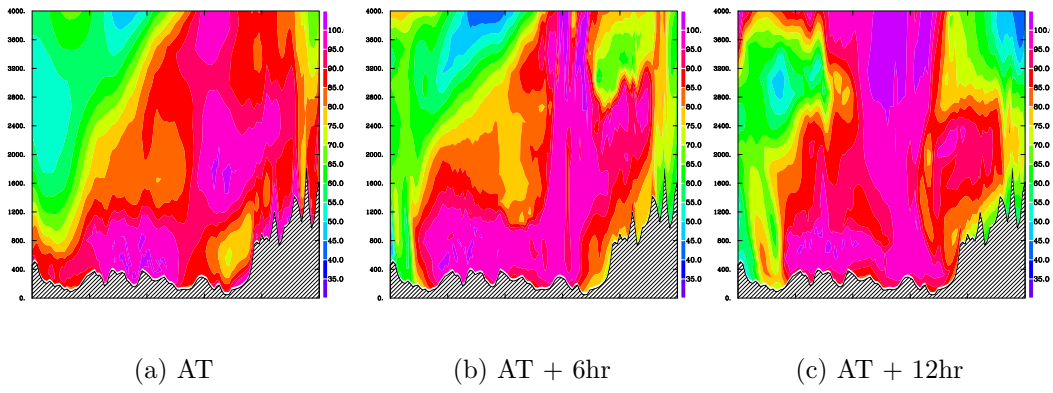


**Figure 16:** Exp. *AA* - Rel. Hum. for a-a'

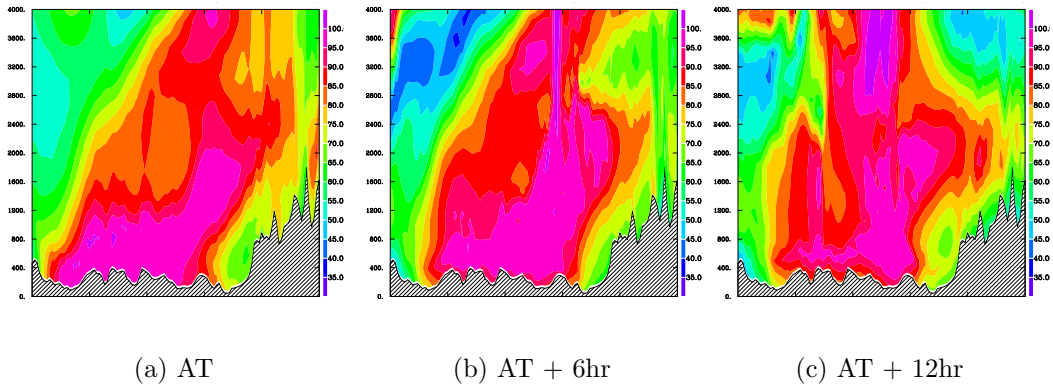


**Figure 17:** Exp. *RR* - Rel. Hum. for a-a'

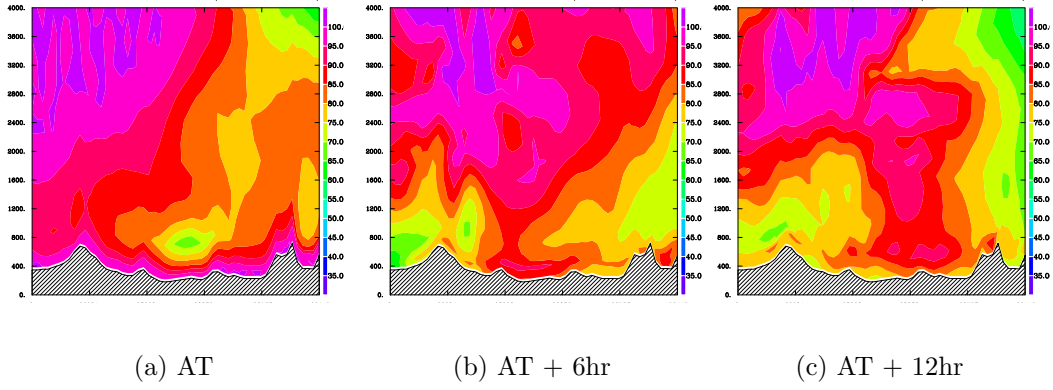


**Figure 18:** Exp. *AA* - Rel. Hum. for b-b'

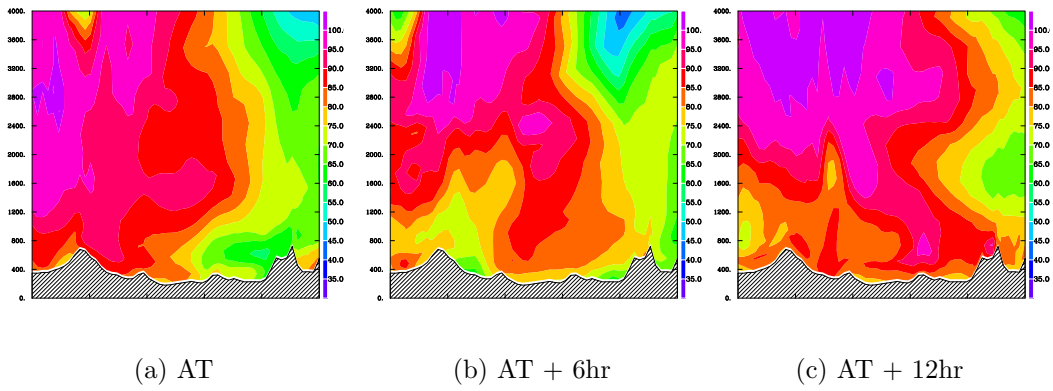


**Figure 19:** Exp. *CC* - Rel. Hum. for b-b'

## 3.2 Radiosonde comparison

Comparisons of models analysis and forecasts with radiosondes messages have been done for three locations: Nîmes–Courbessac<sup>5</sup> (long: 4.40°E, lat: 43.86°N, elev:62m), point **A** of Fig. 3, Lyon–Saint-Exupery (long: 5.08°E, lat: 45.73°N, elev:240m), point **B** and Cuneo–Levaldigi (long: 7.61°E, lat: 44.53°N, elev:386m), point **C**. Upperair data of humidity and temperature are available at analysis time and at  $t + 12hr$  for all the three airports, while wind data only for station **B** and **C**. Fig 20 to Fig. 22 show the profiles of potential temperature, Fig 23 to Fig. 25 the profiles of relative humidity and Fig 27 to Fig. 30 the profiles of wind, both for module and direction.

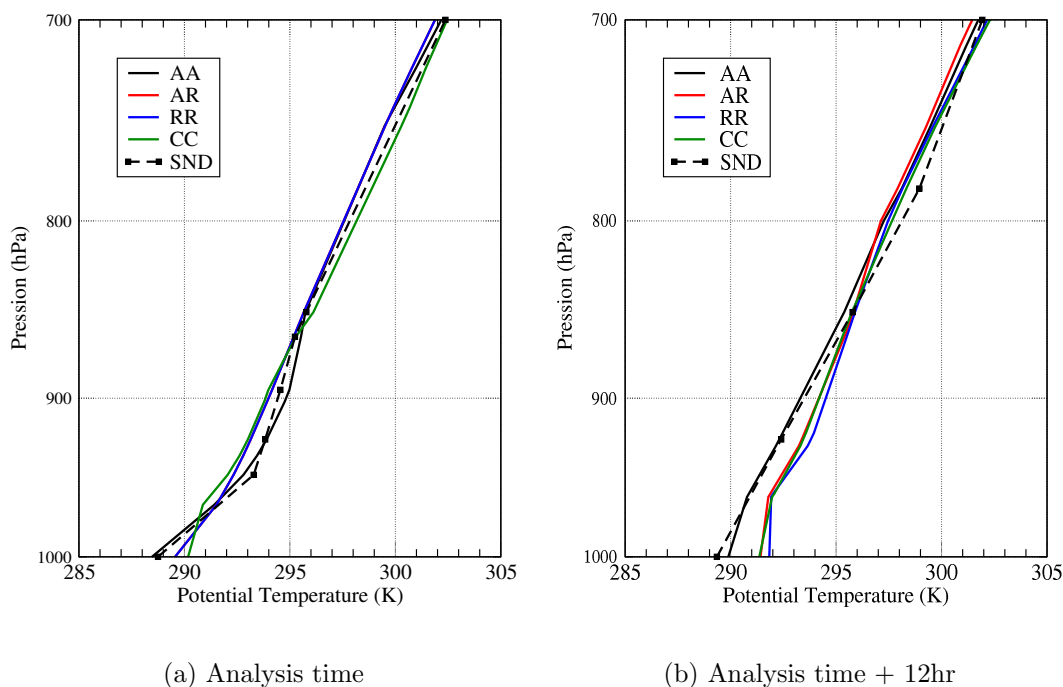
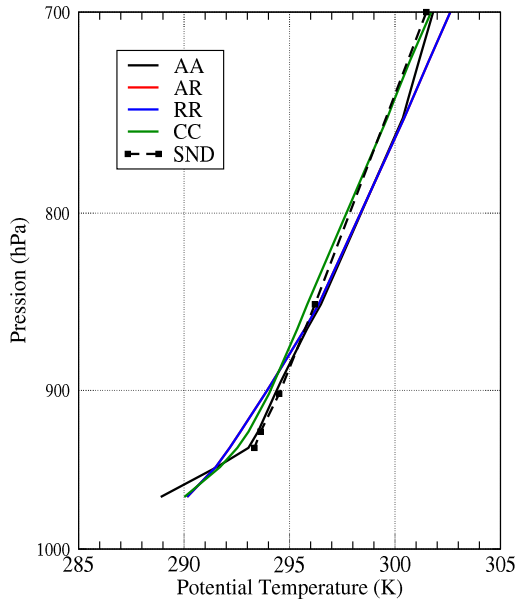


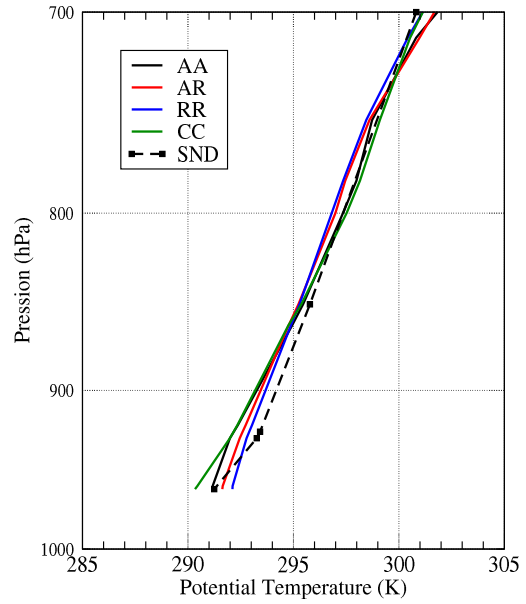
**Figure 20:** Radiosonde comparison for potential temperature at station **A**

Generally speaking, the results show the major capability of Exp. *AA* in analyzing initial conditions of all the quantities. This is true for both surface values and initial gradient. Regarding soundings at station A, the analyzed profile in the 6-hour high-resolution assimilation reproduces the boundary layer state in a better way, according with Sect. 3.1, even if availability of observations only at synoptic hours doesn't permit any analysis about the evolution. At 1200 the difference in temperature is remarkable up to 1.5km of height, reaching 2 degrees at surface level.

<sup>5</sup>This station is located in the center of storm event

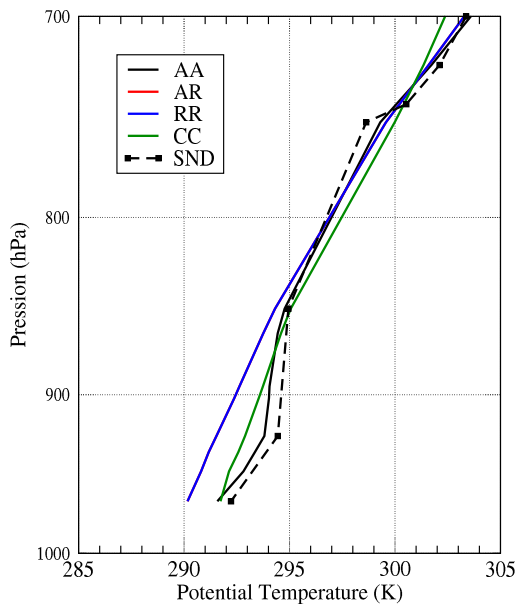


(a) Analysis time

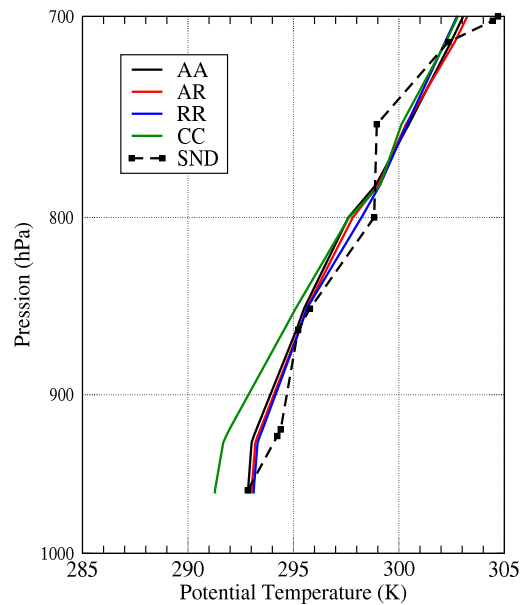


(b) Analysis time + 12hr

**Figure 21:** As in Fig. 20 but for station **B**

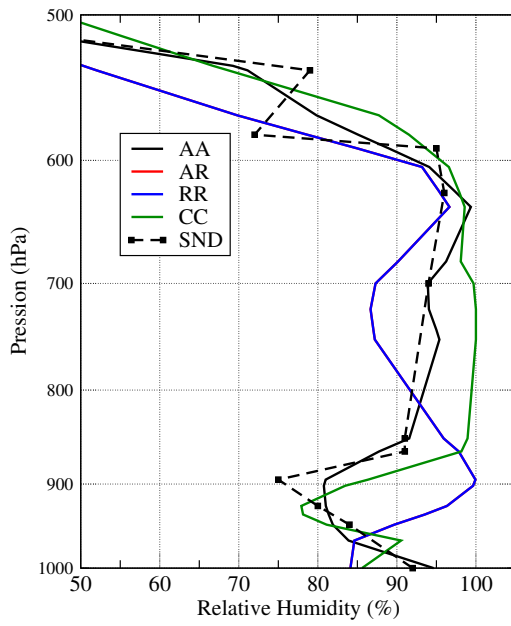


(a) Analysis time

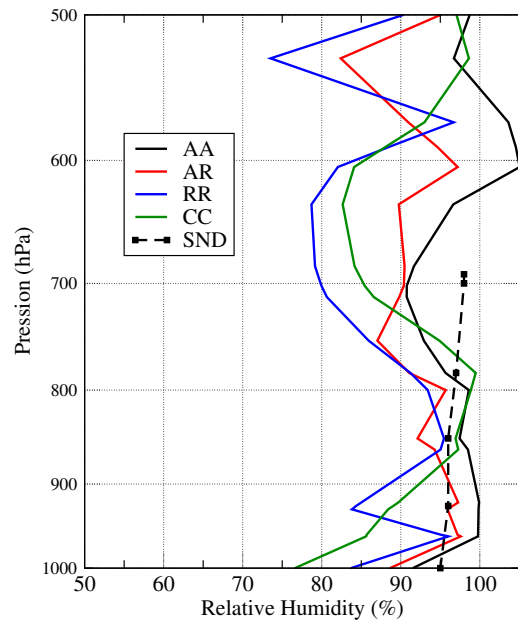


(b) Analysis time + 12hr

**Figure 22:** As in Fig. 20 but for station **C**

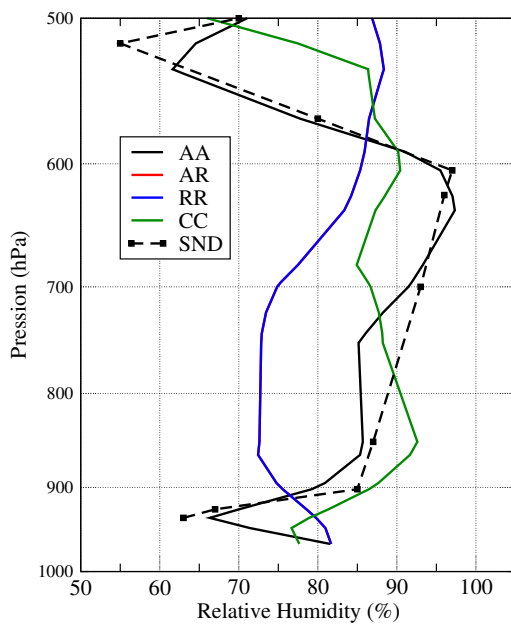


(a) Analysis time

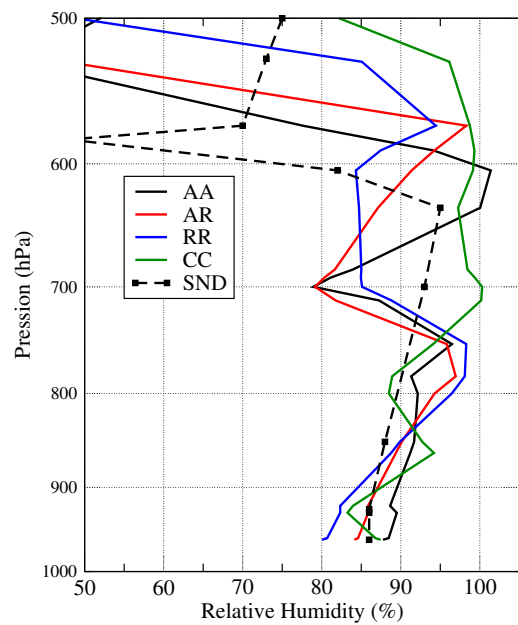


(b) Analysis time + 12hr

**Figure 23:** Radiosonde comparison for relative humidity at station **A**



(a) Analysis time



(b) Analysis time + 12hr

**Figure 24:** As in Fig. 23 but for station **B**

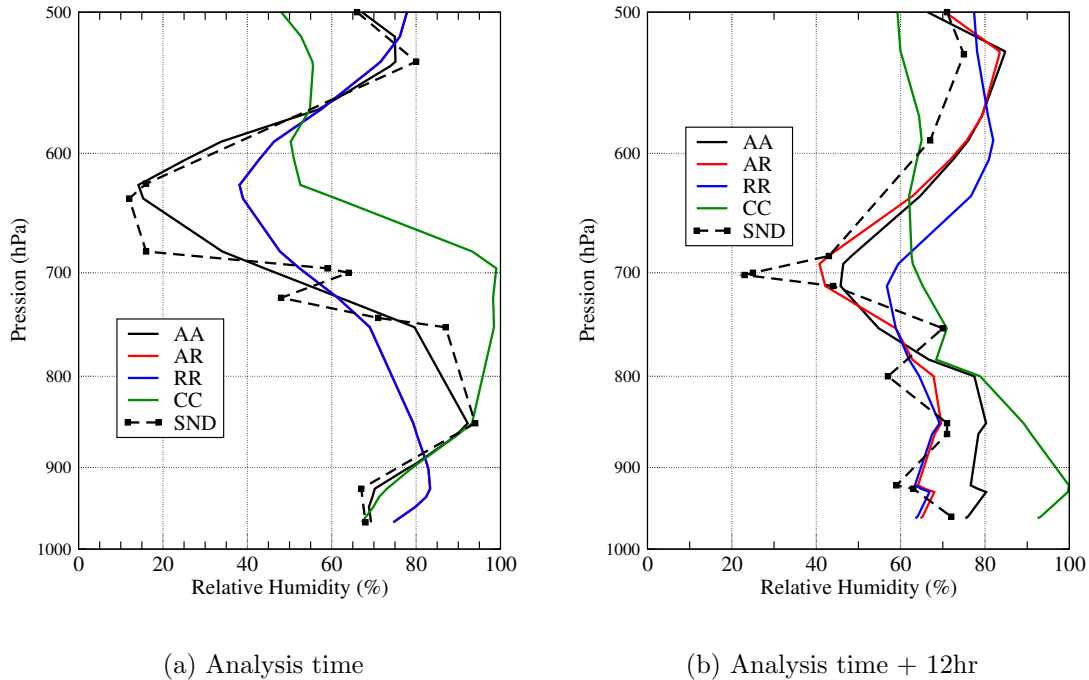


**Figure 25:** As in Fig. 23 but for station **C**

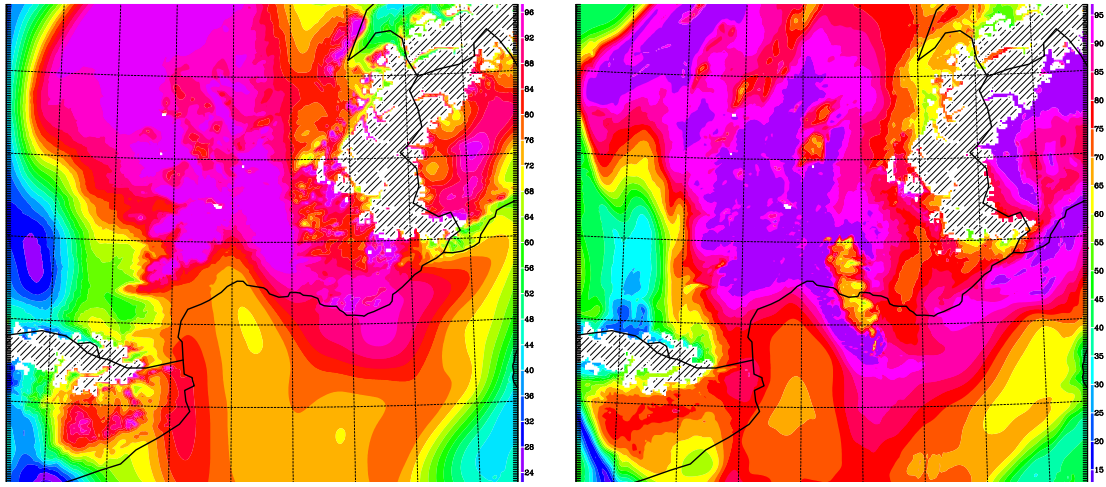
Exp. *CC* seems to overestimate humidity profiles for low and part of middle atmosphere ( $\sim 1km$  to  $5km$ ) in remarkable way at analysis time for station A, as Exp. *RR* presents the opposite behavior. This behavior can be pointed out also examining Fig. 26.

### 3.3 Subjective verification of rainfall

Subjective verification of cumulated rain could be done by comparison of model outputs with observations both from rain-gauge network as well as using radar of Nîmes. Only the outputs from Model 2 are considered.

Fig. 31 to 36 demonstrate the better ability of Exp. *AA* in evaluating cumulated precipitation, in terms of both localization and amplitude. In particular, for the forecast period  $t - t + 6h$  experiments without high-resolution assimilation tend to underestimate the rain over Gard area and neglect precipitation in the northern as well in the southern part of domain (remarkable lack over the Mediterranean Sea in the Gulf of Marseille) and, on the other hand, producing precipitations, not observed, in the north-western one. The cycling experiment results to coarsely overestimate the rainfall event in all the domain.

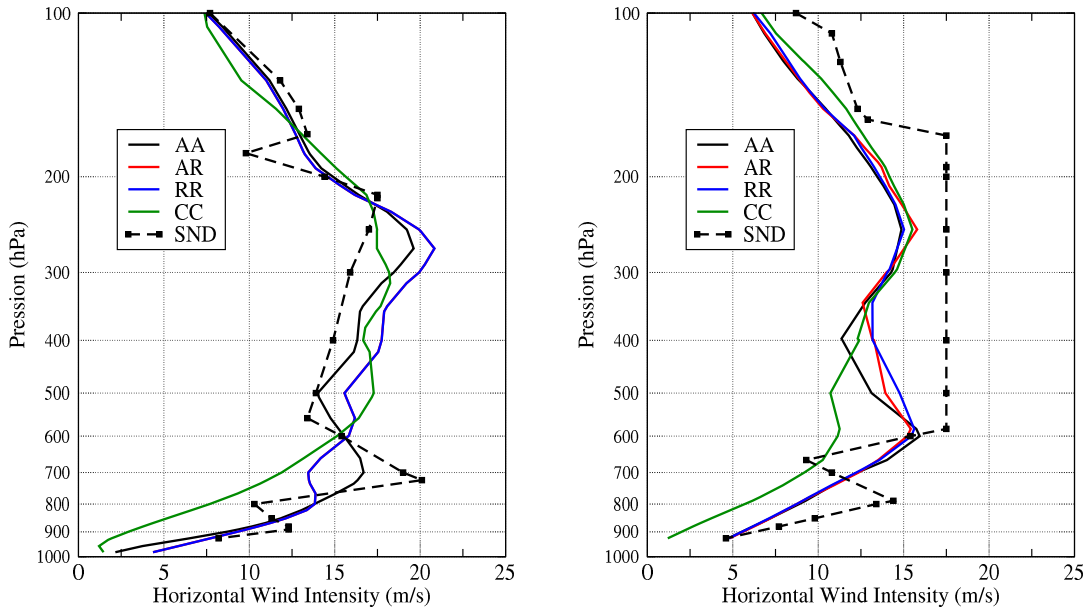
Even for the forecast period  $t + 6h - t + 12h$  the Exp. *AA* better hits rain fields, but here the differences with Exp. *AR* and Exp. *RR* are less marked. Furthermore,



(a) Exp. AA

(b) Exp. CC

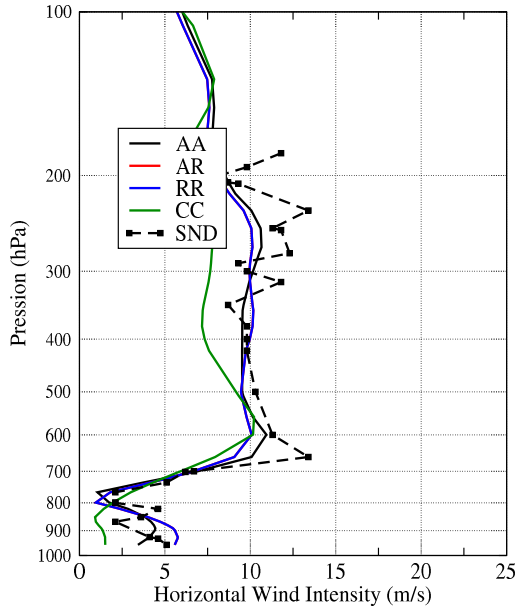
**Figure 26:** Relative Humidity at Z=1500m



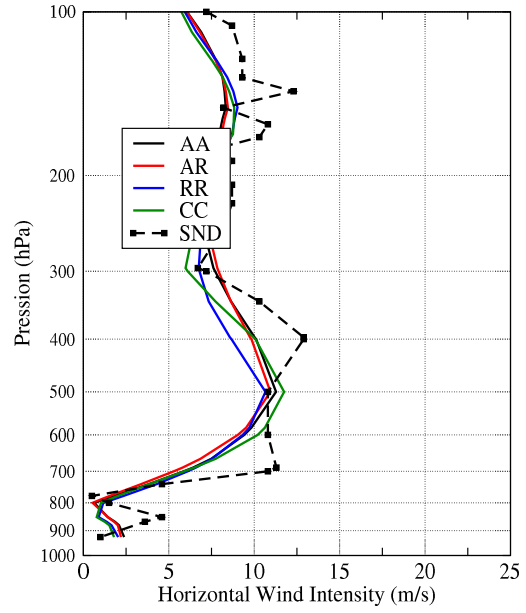
(a) Analysis time

(b) Analysis time + 12hr

**Figure 27:** Radiosonde comparison for wind module at station B

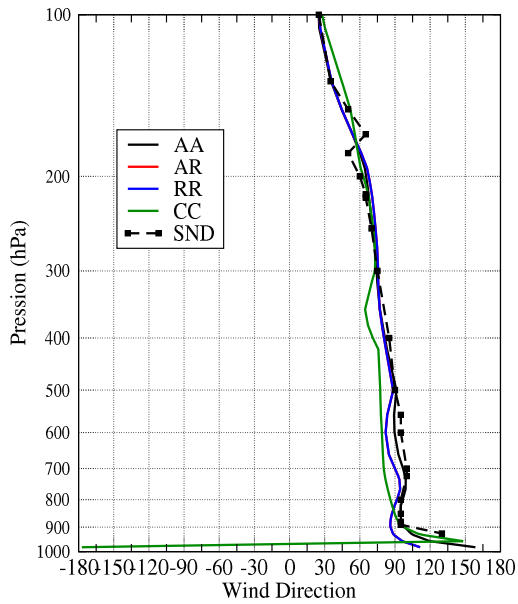


(a) Analysis time

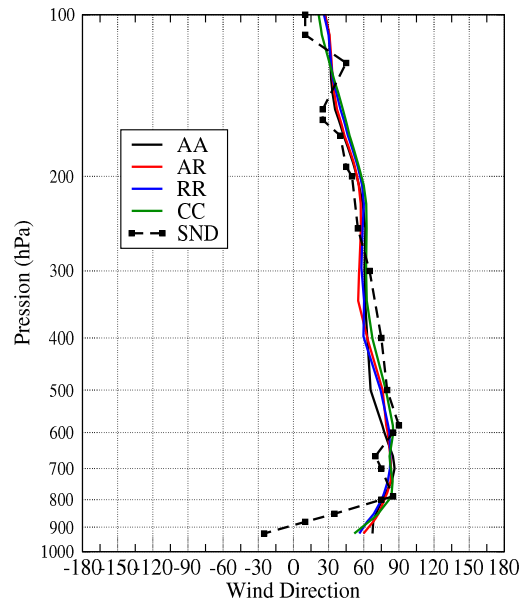


(b) Analysis time + 12hr

**Figure 28:** As in Fig. 27 but for station C



(a) Analysis time



(b) Analysis time + 12hr

**Figure 29:** Radiosonde comparison for wind direction at station B

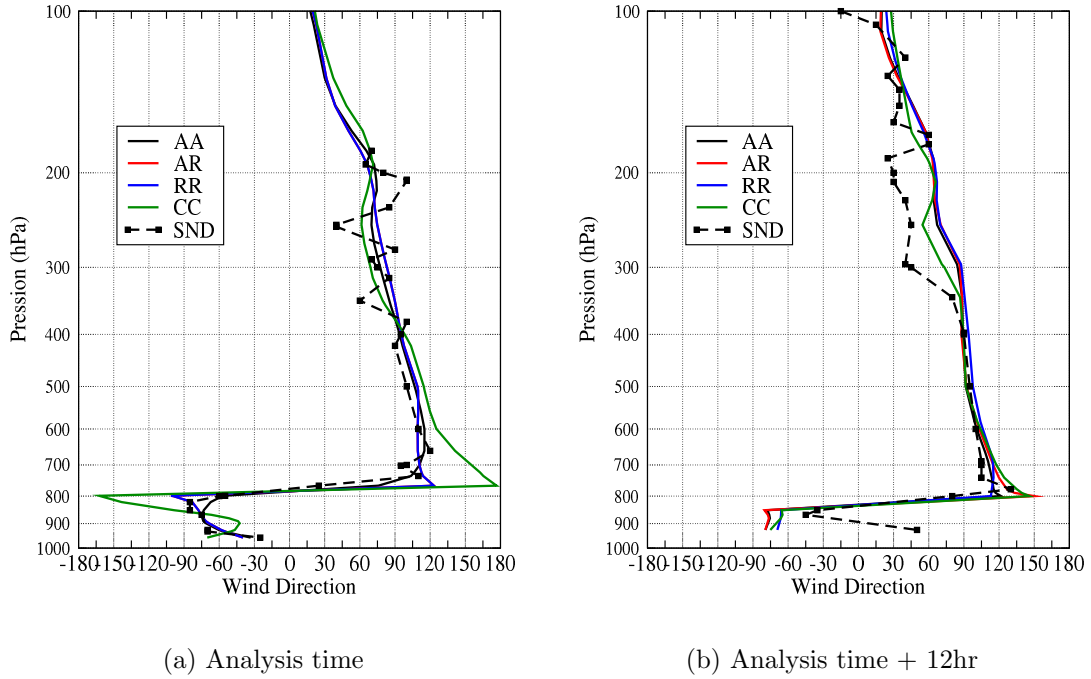


Figure 30: As in Fig. 29 but for station C

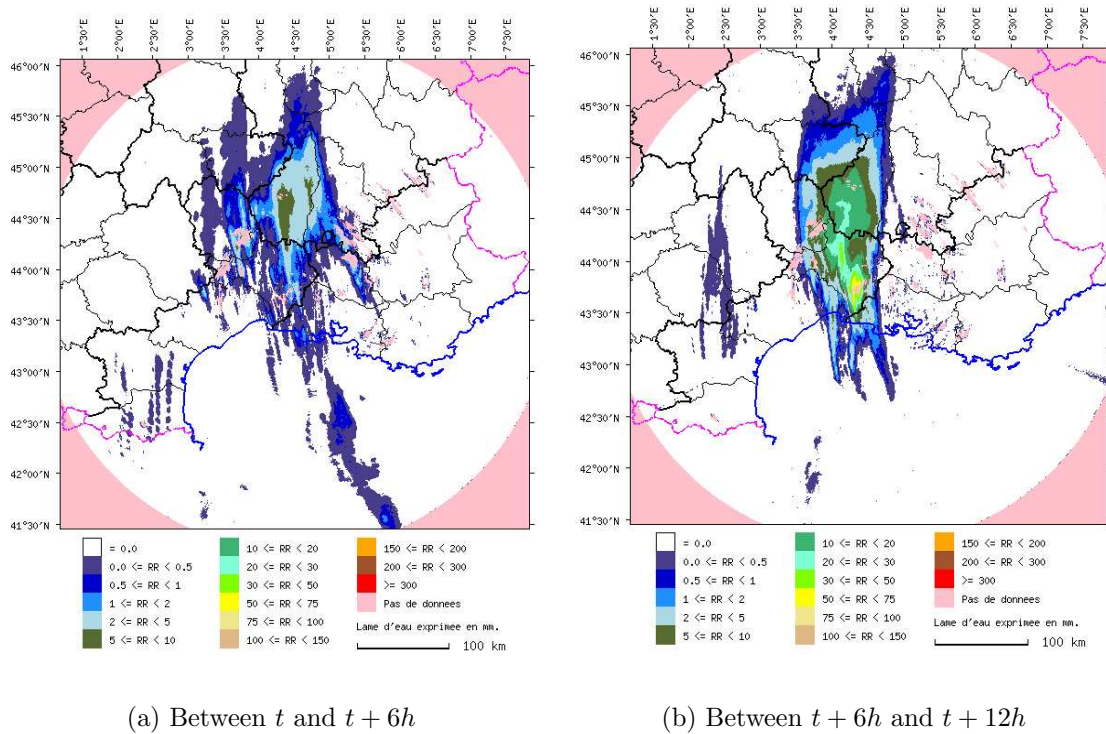
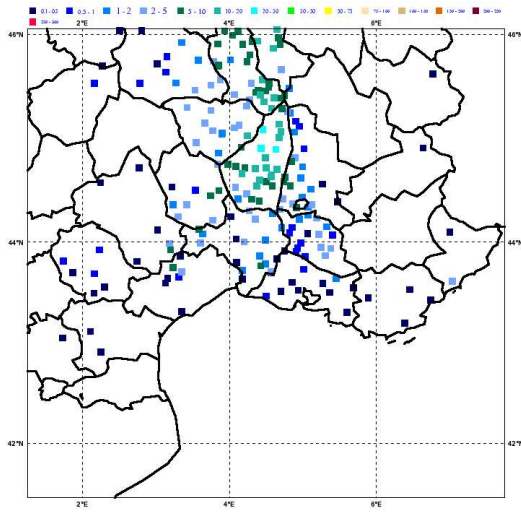
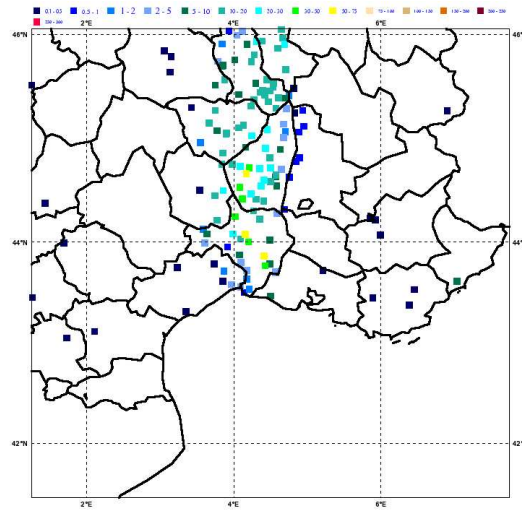


Figure 31: 6hr cumulated rain as observed from meteorological radar of Nîmes

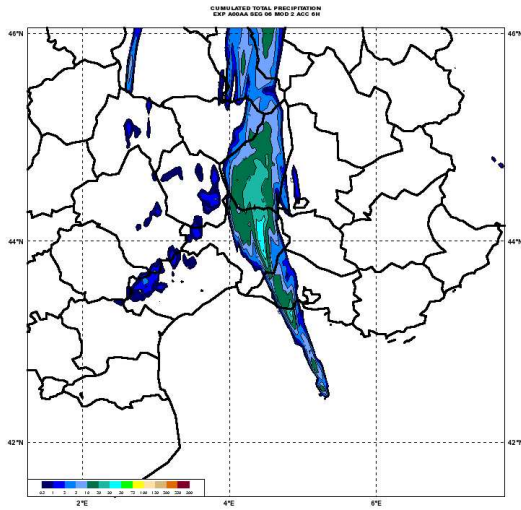


(a) Between  $t$  and  $t + 6h$

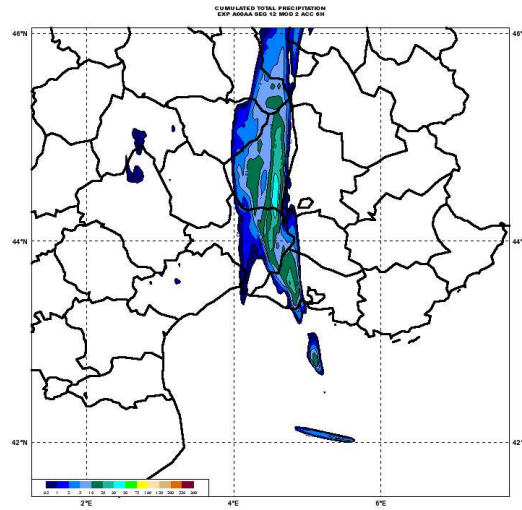


(b) Between  $t + 6h$  and  $t + 12h$

**Figure 32:** 6hr cumulated rain as observed from rain-gauge network

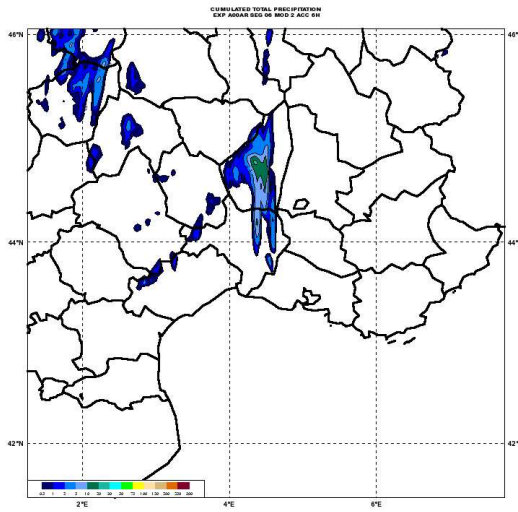


(a) Between  $t$  and  $t + 6h$

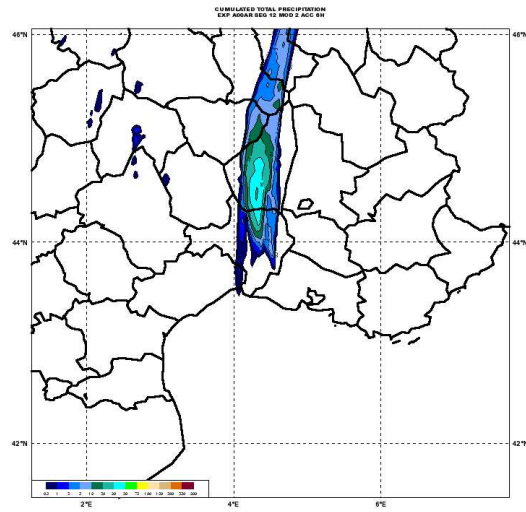


(b) Between  $t + 6h$  and  $t + 12h$

**Figure 33:** 6hr cumulated rain for Exp. AA

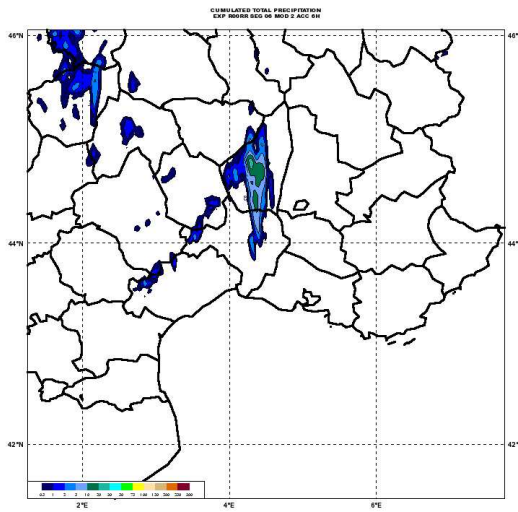


(a) Between  $t$  and  $t + 6h$

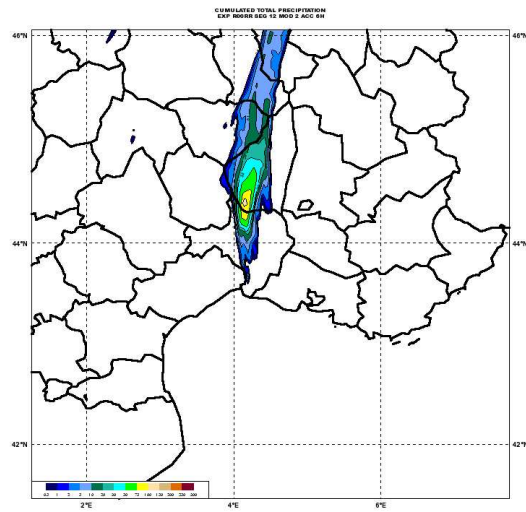


(b) Between  $t + 6h$  and  $t + 12h$

**Figure 34:** 6hr cumulated rain for Exp. *AR*

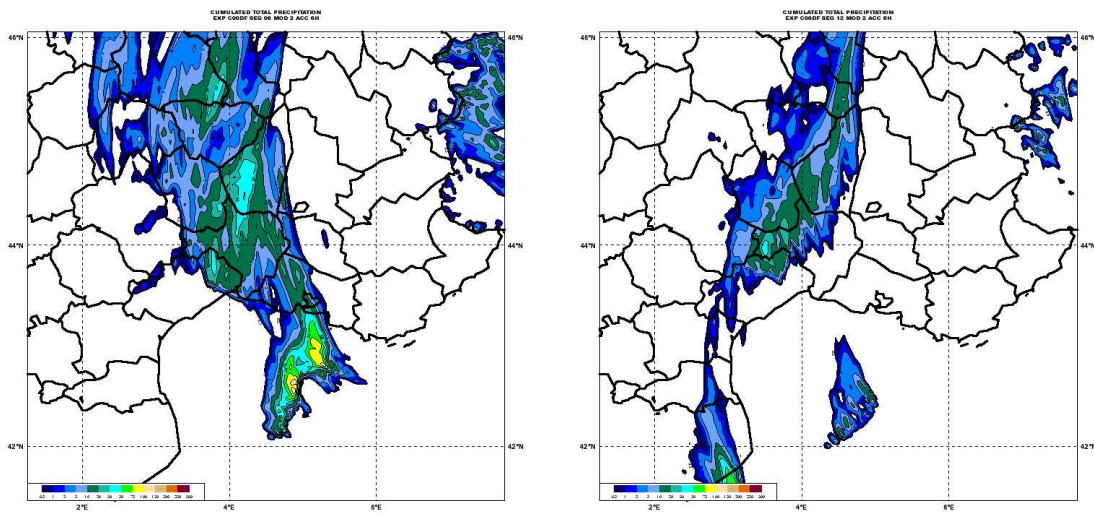


(a) Between  $t$  and  $t + 6h$



(b) Between  $t + 6h$  and  $t + 12h$

**Figure 35:** 6hr cumulated rain for Exp. *RR*



(a) Between  $t$  and  $t + 6h$

(b) Between  $t + 6h$  and  $t + 12h$

**Figure 36:** 6hr cumulated rain for Exp. *CC*

these simulations succeed to get real value of maximum intensity rain (up to  $70 \text{ mm} \cdot 6\text{hr}^{-1}$ ) in Gard area. An interesting evidence is that the more resolution of assimilation increases the more rain distribution correctly moves easternwards. Finally, Exp. *CC* presents precipitation value also after just an hour of forecasting (Fig. 37) while available data do not show it. It may be explained as a typical spin-up problem (Dance, 2004).

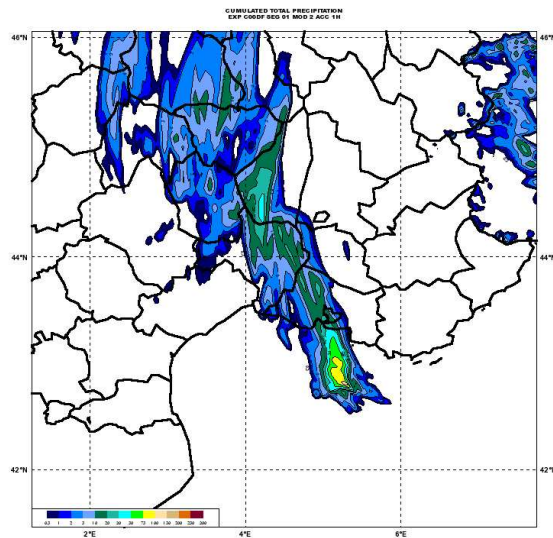


**Figure 37:** Cumulated rain for Exp. *CC* in the first hour of forecasts.

### 3.4 Verification of surface quantities by scores comparison

Mean Error (**ME**) and Mean Squared Error (**MSE**)<sup>6</sup> have been computed. The following figures (38 to 43 exhibit the temporal evolution of errors, and a linear fitting is imposed in the Forecasts versus Observation diagram in order to visualize the errors in function of ranges.

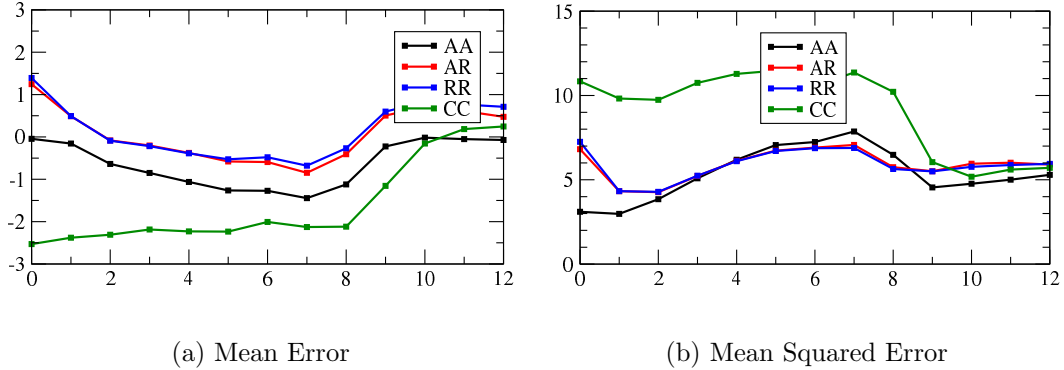


**Figure 38:** Error statistics versus time for 2-meters temperature

For humidity and temperature at 2 meters a.g.l., Exp. *AA* always results in best accordance with observations. Tendency of Exp. *CC* is to undervalue surface temperature and overestimate humidity (see Fig. 44). All the experiments anyway overestimate 2 m temperature on the average for the first hours of forecasting. Less remarkable is the differences for what regards wind errors, that is underestimate for all the experiments.

### 3.5 Verification of QPFs by scores comparison

Verification of QPFs have been carried out using traditional statistics (Thornes and Stephenson, 2001; Wwrp/Wgne, 2004). While the improvements in terms of scores are often not obvious in model inter-comparison (Ebert et al., 2003), they help in understanding the trends of the experiments and provide more rigorous evidences yet achieved by subjective verification, even if recent studies have pointed out how scores have some problems in meso-gamma applications for reasons of both interpolation (Accadia et al., 2003) and resolution (Hamill and Juras, 2005). According to Nurmi (2003), Tab. 3 considers, for every chosen threshold (see Tab. 4), four possibilities which come out from comparison between observations and models

<sup>6</sup>ME is defined as  $(1/n) \sum_i (f_i - o_i)$  while MSE as  $(1/n) \sum_i (f_i - o_i)^2$ . The first one gives a measure of averaged total error but it can neglect amplitude error, anyway present for MSE statistic

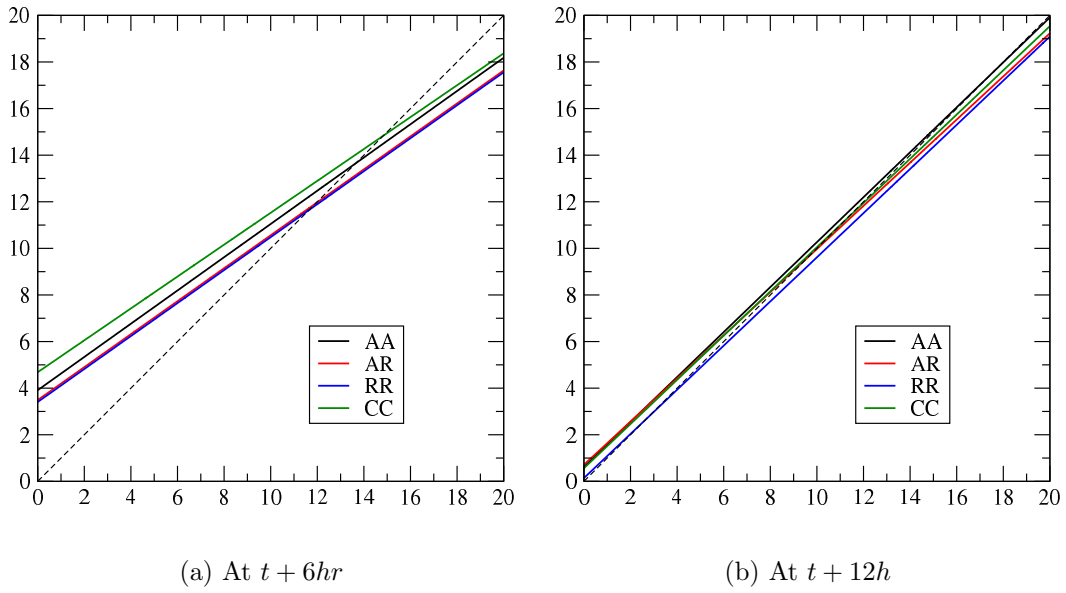


**Figure 39:** Observations (x-axis) vs Forecasts (y-axis) linear fitting for 2-meters temperature

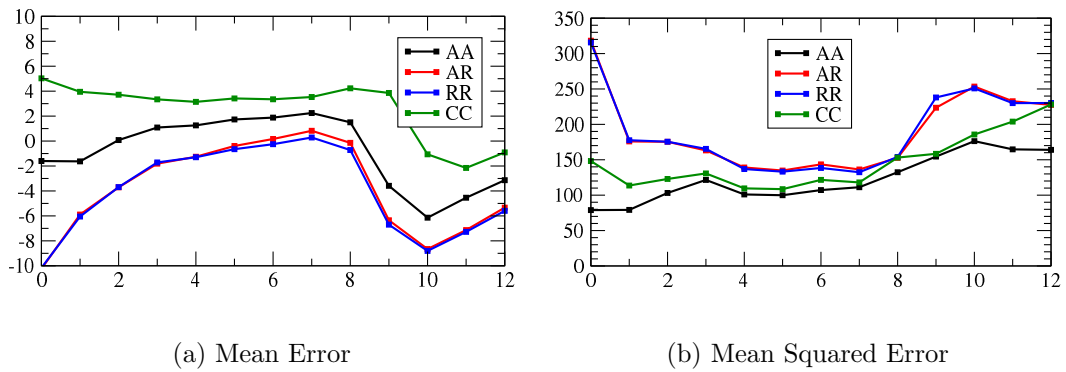


**Figure 40:** As in Fig. 38 for 2-meters relative humidity

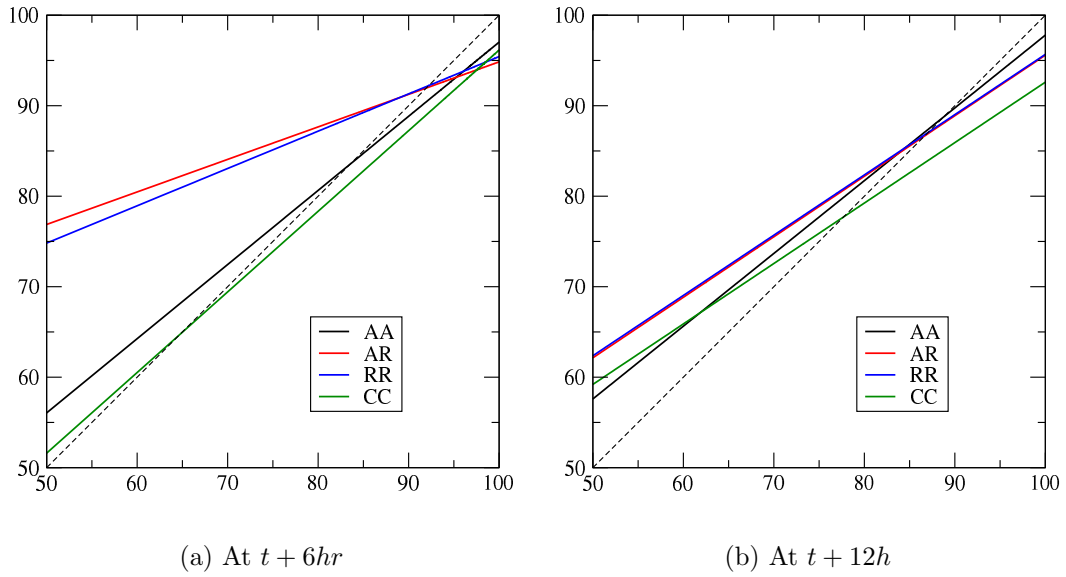


**Figure 41:** As in Fig. 39 for 2-meters relative humidity

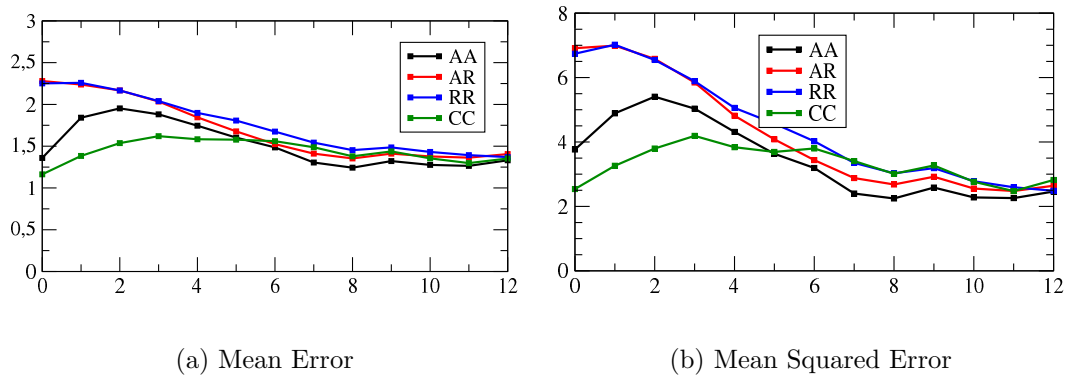


**Figure 42:** As in Fig. 38 for 10-meters horizontal wind intensity

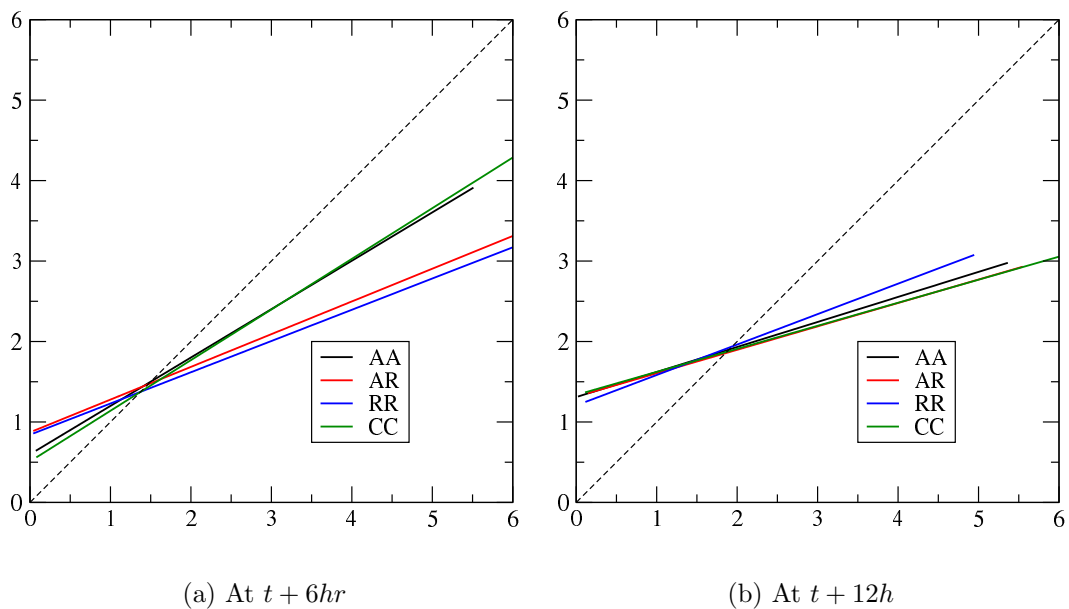


**Figure 43:** As in Fig. 39 for 10-meters horizontal wind intensity

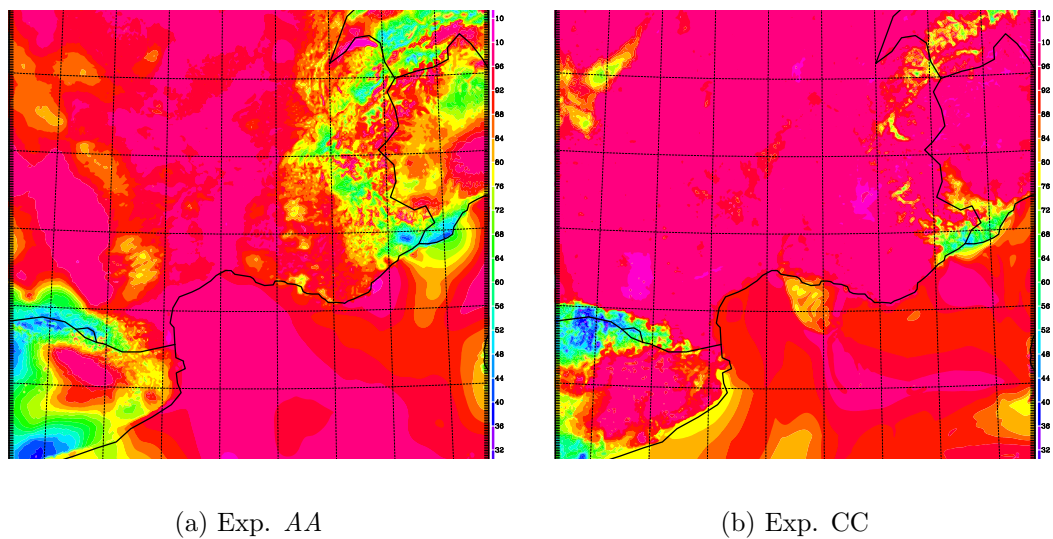


**Figure 44:** 2-meters relative humidity fields at analysis time

forecasts. The method is to interpolate the models output to stations points, since the high resolution can preserve results from smoothing errors (Cherubini et al., 2002). This comparison is made with rain-gauge measurements, whose French observing network is showed in Fig. 45, consisting of 685 stations inside the Model 2 domain.

		Observation	
		Yes	No
Forecast	Yes	Hit ( <i>a</i> )	False alarm ( <i>b</i> )
	No	Miss ( <i>c</i> )	Correct rejection ( <i>d</i> )

**Table 3:** Contingency table for skill scores

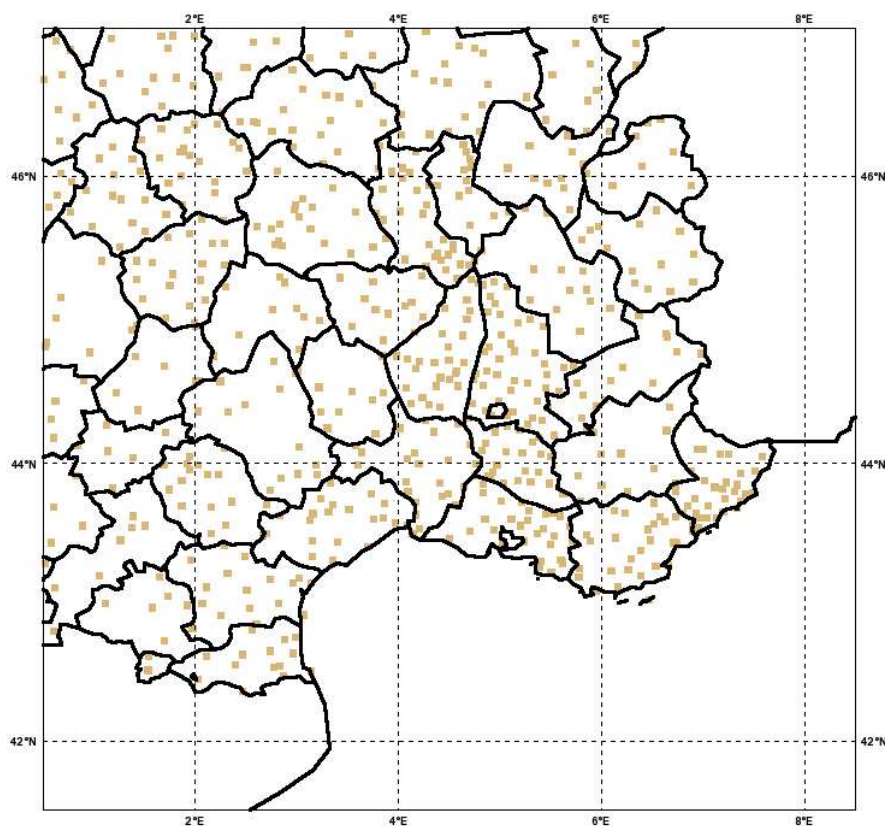


**Figure 45:** Dissemination of rain-gauge measurements

Cumulated rain in $mm \cdot 6hr^{-1}$					
0.5	2	5	10	20	30

**Table 4:** Thresholds used in quantitative precipitation forecasts scores

The computed scores are **Accuracy**, defined as:

$$ACC = \frac{a + d}{a + b + c + d} \quad (1)$$

which is the ratio between the correct forecasts and all the forecasts; the **Probability of Detection** (POD),

$$POD = \frac{a}{a + c} \quad (2)$$

whose meaning is to evaluate the well-forecasted events exceeding the threshold; the **False Alarm Rate** (F)

$$F = \frac{b}{a + b} \quad (3)$$

that is a measure of occurrences for which precipitation is not stronger than the value taken into account; the **Frequency Bias** (FB), to compare the frequency of forecasts to the frequency of observed occurrences:

$$FB = \frac{a + b}{a + c} \quad (4)$$

Further to these ones, one more score has been calculated, the **Equitable Threat Score** (ETS), which is sensitive to the number of hits compared to the number of false alarm and misses

$$ETS = \frac{a - a_r}{a + b + c - a_r} \quad (5)$$

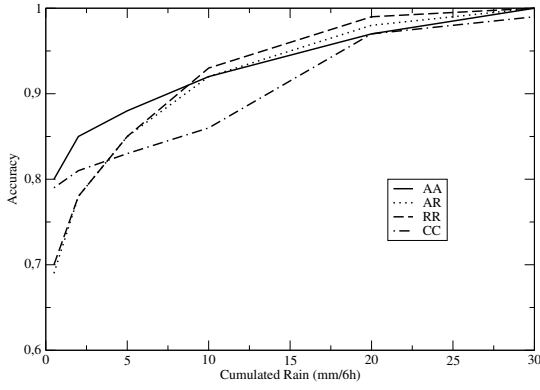
where  $a_r$  represents the number hits for random chance:

$$a_r = \frac{(a + b)(a + c)}{n} \quad (6)$$

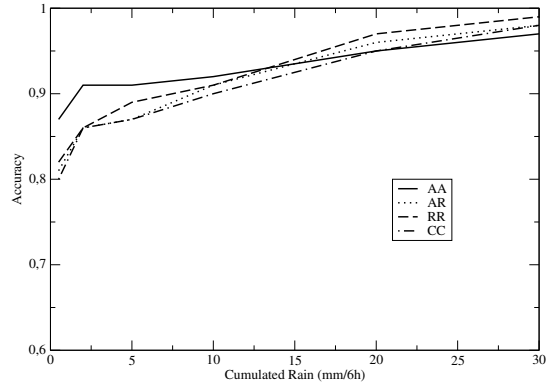
ETS ranges from  $-\frac{1}{3}$  to 1; perfect scoring is 1.

Results show that the overall accuracy is greater for Exp. *AA*, at least for all the rainfall events not stronger than  $20 \text{ mm} \cdot (6\text{hr})^{-1}$ . The cycling experiment doesn't perform correctly the QPFs, in comparison with others, since it produces an overestimate for all the precipitation thresholds, while the two reference experiments (*RR* and *AR*) present very similar behaviors and generally underestimate rain quantities, keeping a lower rate of false alarms, even if the differences in terms of FAR are greater for the first thresholds, where the importance itself of not detecting false alarms is secondary.

In absolute terms, better accuracy is achieved during the second six hours for all the experiments but the *CC*, where the rate of false alarms gets slightly smaller.

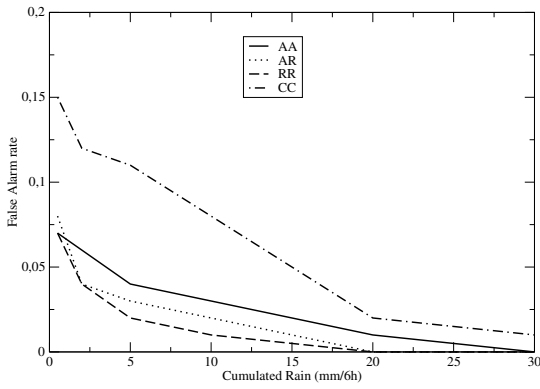


(a) Between  $t$  and  $t + 6h$

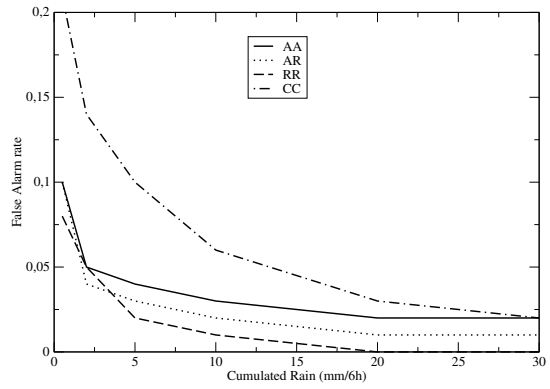


(b) Between  $t + 6h$  and  $t + 12h$

**Figure 46:** Accuracies of quantitative precipitation forecasts

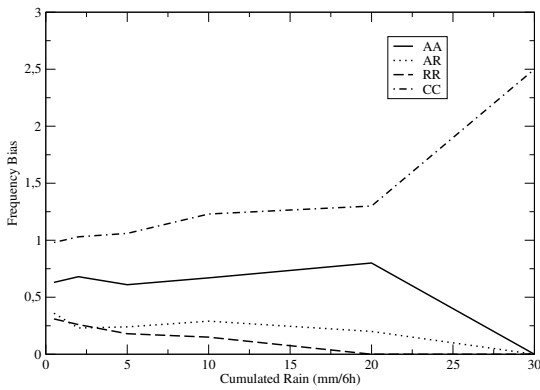


(a) Between  $t$  and  $t + 6h$

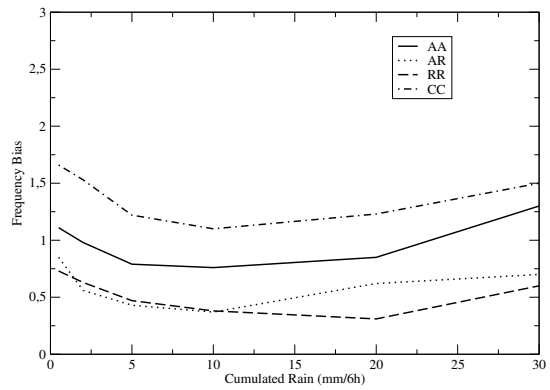


(b) Between  $t + 6h$  and  $t + 12h$

**Figure 47:** False Alarm Rates of quantitative precipitation forecasts



(a) Between  $t$  and  $t + 6h$



(b) Between  $t + 6h$  and  $t + 12h$

**Figure 48:** Frequency biases of quantitative precipitation forecasts

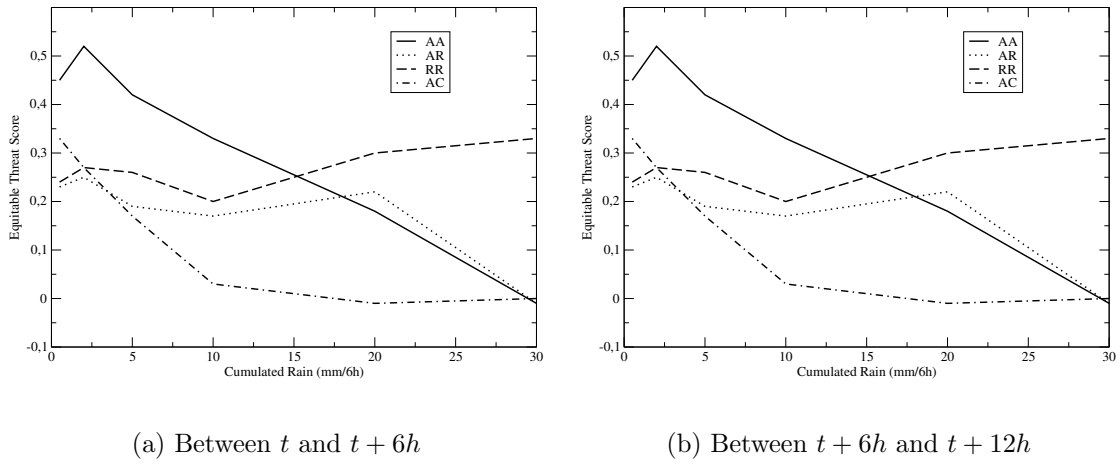


**Figure 49:** Equitable Threat Scores of quantitative precipitation forecasts

Additionally, the FR versus POD diagram, where FR is the **False Alarm Ratio**<sup>7</sup>, proves that for the  $12h - 6h$  cumulated rain there are more difficulties in evaluating different tendencies of the experiments, since the behavior is not coherent with the thresholds.

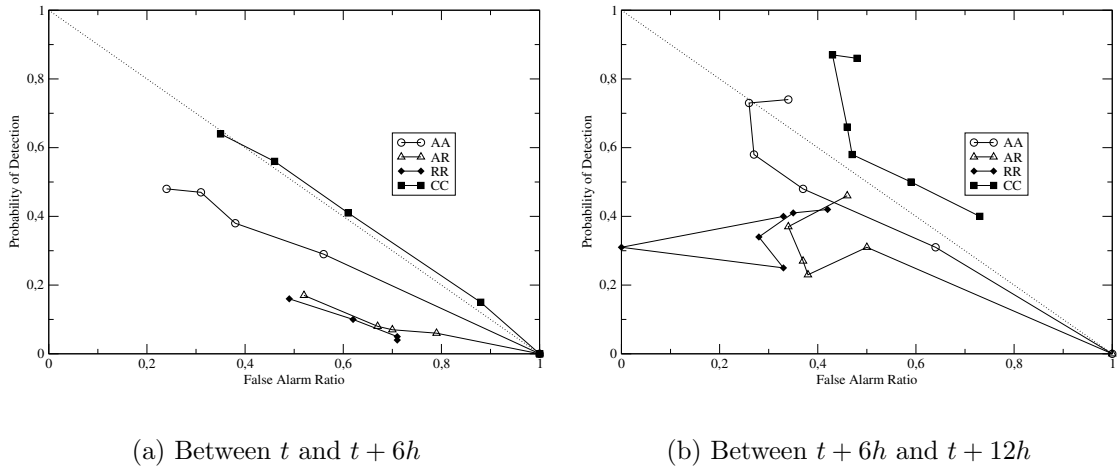


**Figure 50:** POD vs FAR diagrams

<sup>7</sup>The False Alarm Ratio, to not mistake for the False Alarm Rate, is defined as  $\frac{(a+b)(a+c)}{n}$  and it's sensitive to false alarms but not to misses like POD. So, since when one increases the other too, examining them together lets understand if models errors are equilibrated or rather there are overestimating tendencies.

## 4 Conclusions

A strong precipitation event over the French Languedoc region has been simulated using an high-resolution 3D-Var assimilation to accompany with the operational meso-beta scale of assimilation. All the verification systems show the better capability of this experiment to analyze humidity and temperature fields, for what regarding the analysis as well the forecasts. This feature is retrieved in terms of both localization and quantitative forecasting of precipitation. To be precis, around Nîmes, where is localized the maximum value of daily precipitation, radiosonde measurements agree with increased humidity achieved at first model vertical levels by Exp. AA. Such an increase, whose role in development of storm is basic, is not detected by other experiments. For the same area, a in a similar way it has been founded the better accuracy for what concerning gradient and values of temperature. Furthermore, all the scores of surface quantities and cumulated rain are favorable to this method. The background error covariances augmented at low-levels, the assimilation of a well-disseminated network of observations at 2 meters, further to the meso-gamma scale of analysis seem to be concomitant contributors to the result, and their relative impact is hard to find.

Use of MSG/SEVIRI radiances in the hope of recover the lack of humidity data for upperair atmosphere has had no positive impact on analysis, since an overestimate of humidity, mainly for the low atmosphere over Mediterranean coast produced bigger values for precipitation and enlarged the area hit by rainfall. Experiment with an hourly time-step of assimilation has demonstrated to need additional studies, whereas it seems to be invalidated by a spin-up behavior – rainfall is present also in the first hour of forecasting while there’s no evidence. Hence, the impact of background errors should be investigated more deeply. Anyway, in this cycling experiment the observations at 2 meters could not be used, since a problem in the passage from the space of observations to the model space, given fixed value for ground temperature and at surface, produced unrealistic increments, and a posteriori analysis of these two temperature is not able to recover it. Since the difficulties of a practical implementation of the surface and the deep analysis inside 3D-Var computations, it could be suggested to define a preliminary analysis for these temperatures in order to limit the contrast in the minimization procedure.

## A Assimilation of 2m temperature for cycling experiment

While assimilation of temperature and humidity data at 2 meters a.g.l. gave interesting results for cold-start experiment with assimilating time-window set to six hours, the choice of avoiding use of these observations in the 1-hour cycling experiment is due to the evidence of errors in analyzed temperature fields, at least for the first 6 model vertical levels (see Fig. 51 where increments reach up to 6 degrees for the first model level). In fact, analysis model has been not able to use correctly this information inside the gridded analyzed fields of temperature.

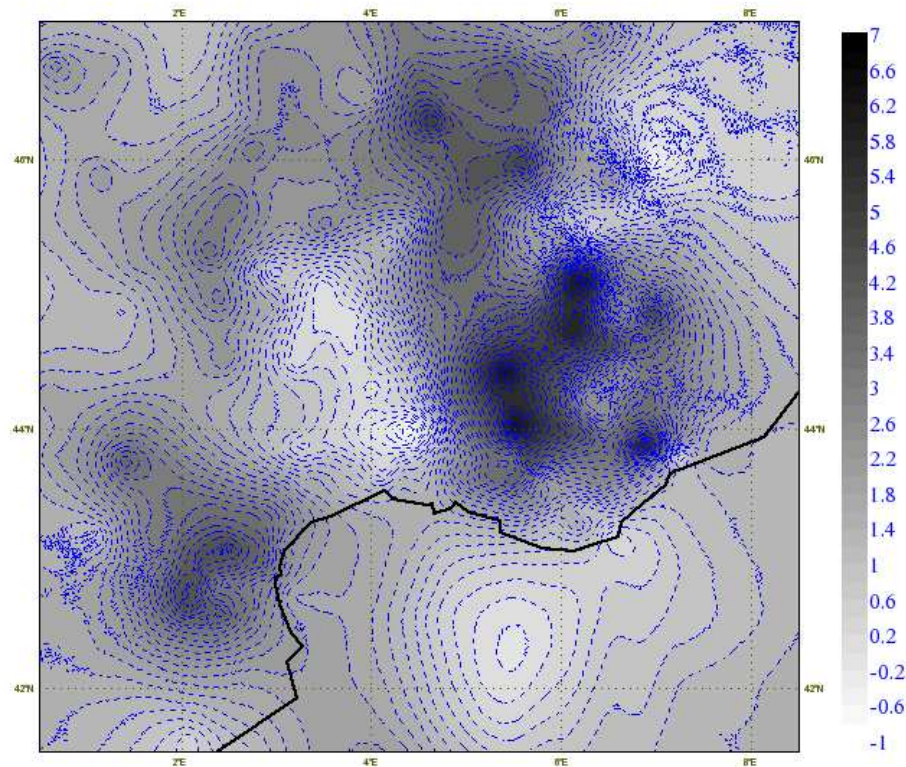


**Figure 51:** Increments of  $T_{41}$  at 09 p.m. for cycling experiment with 2-meters humidity and temperature assimilation

As showed in Fig. 52 that summarizes results of minimization between 08 p.m. and 09 p.m. of 3-11-2004 for experiment with 2-meters data assimilation, 77% of innovations is between -2 and +2 degrees and this range arrives to 84% of occurrences after minimization. This result evidently doesn't justify the analyzed field of temperature for the first model level (see also the different profiles of temperature showed in Fig. 52(a) and (b) ). Furthermore, this different analysis produces super-adiabatic profiles which strongly influence all the fluxes and wind fields because of

the new thermal forcing, and causing a general overestimate of rainfalls.

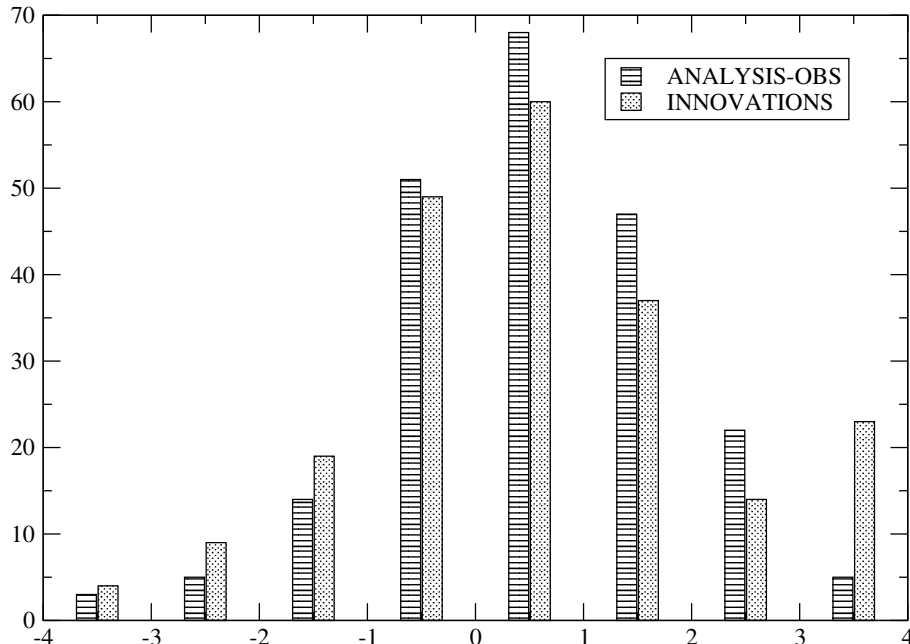


**Figure 52:** Range of innovations and increments for the same analysis of Fig. 51

Results are due to the fact that analysis projects 2-meters increments in the model-space, without modifying former values of superficial temperature and ground temperature. So, given values of temperature at surface, underground and at 2 meters above ground level, the temperature in the first levels are modified to obtain a continuous temperature profile coherent with these values. As the innovation is large enough (for instance in the case it ranges between 1 and 2 degrees) the  $T_{41}$  to  $T_{35}$  can grow up to 6 degrees. Activating a rejecting procedure, no 2-meters data are accounted for in the minimization task; on the other hand, modifying  $J_B$  in order to not exalt low-levels data (see B), has no remarkable influence on the analyzed fields of temperature. Neither the inclusion of an independent surface analysis task<sup>8</sup> to modify surface values are not capable to arrange the  $T_{41}$ 's increase, since, for what formerly explained, this depends on the inside of the minimization procedure and a posteriori modification does not consider errors in  $T_{41}$  and closer levels.

Such a problem is not noticed in the Exp. *AA*, where the 6 hours time-window – with the cold-start initialization – seems to be large enough to take into account the 2 meters observations with a not very big innovation value (in this case screening

<sup>8</sup>In this case, after 3D-Var analysis, the ground temperature  $T_D$  and the surface temperature  $T_S$  are modified to take into account low-levels observations also for these quantities, not incremented during minimization. For ground temperature  $T_D^{SA} = T_D^A + \frac{T_{41}^A - T_{41}^B}{6}$ , while for surface temperature  $T_S^{SA} = T_S^A + (T_{41}^A - T_{41}^B)$ , where over-scripts *SA*, *A* and *B* mean to say Surface Analysis, Analysis and Background respectively.

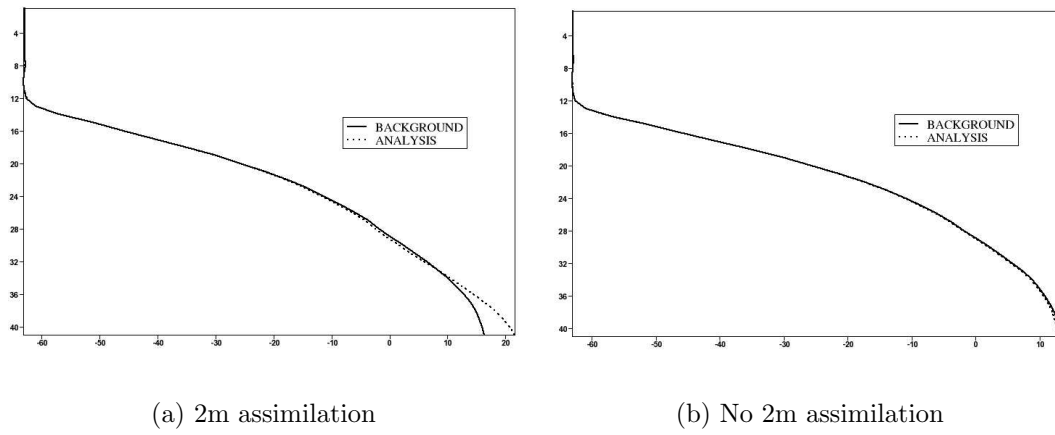


**Figure 53:** Profiles of temperature for cycling experiments at 09 p.m.

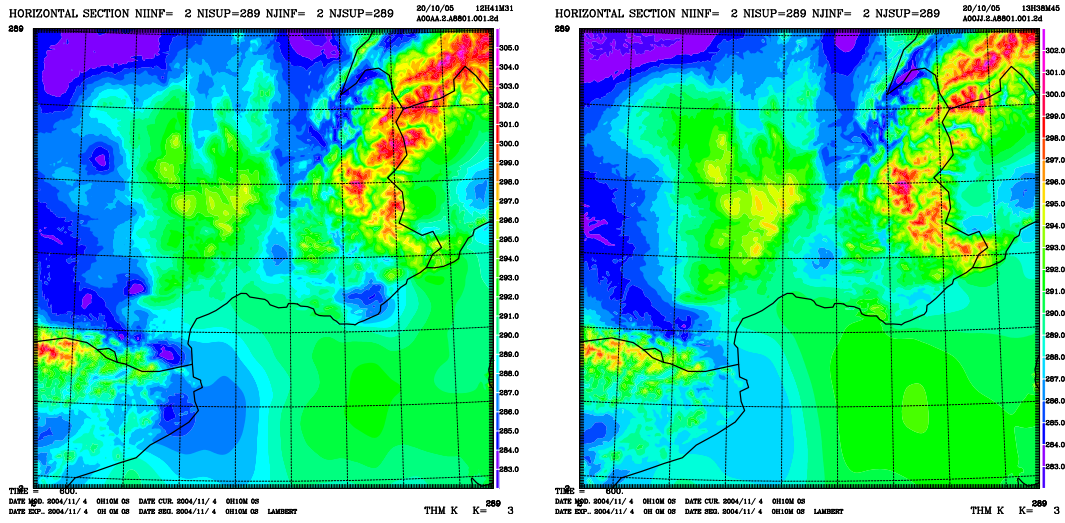
procedure is active) and to produce reasonable values of  $T_{41}$  field, considering that there's no forecasting task in the assimilation cycle.

## B The error background covariances used in the simulations

The definition of background errors for high-resolution model is a delicate question, whereas they have to be taken into account simultaneously different scales of constraints and different spatial and temporal correlations for observed data. For this reasons using a static structure of background error could result wrong in a limited area model, on the contrary it doesn't need additional computational expense. In these experiments error background covariances are obtained from the operational Aladin error statistics. These ones result from application of an ensemble method for which observations are randomly perturbed and the differences between analysis represent the error evolution, in order to better estimate statistics depending on the quality and dissemination of data (Belo Pereira and Berre, 2005). To reach up the requested high-resolution for the experiments, two  $J_B$  coming from different procedures are utilized: A)<sup>9</sup> Starting from a 30km-resolution ensemble  $J_B$ , it is interpolated in the new domain and his variances are increased, mainly for low-levels; B) As A but without augmented variances. Precedent tests had showed how A succeeded rather than B in getting analysis increments closer to observations. Moreover, the influence of a surface observation of humidity or temperature in terms of auto-correlation extends larger. Anyway, this choice allows, generally speaking, a minimization procedure in which analysis was theoretically closer to observations in respect to B, so, considered the problems with 2 meters observations (App. A) and the possibility of lack of information in the hourly cycle assimilation, analysis has been conducted also with B, for both the experiments. Problems in 2 meters observations assimilation do not depend on error background covariance, so comparison between Exp. *CC* and *CJ* is not interesting. The only comment that one wants to do, since a study on the influence of error background structure would require an ad hoc analysis, regards humidity and potential temperature field at the first model level. Using a B  $J_B$  with no variances augmented lets the analysis partially neglect the anomalous increase of humidity in the Gard area, nullifying the benefits of a high-resolution assimilation in a frame of abundance of surface observations.

---

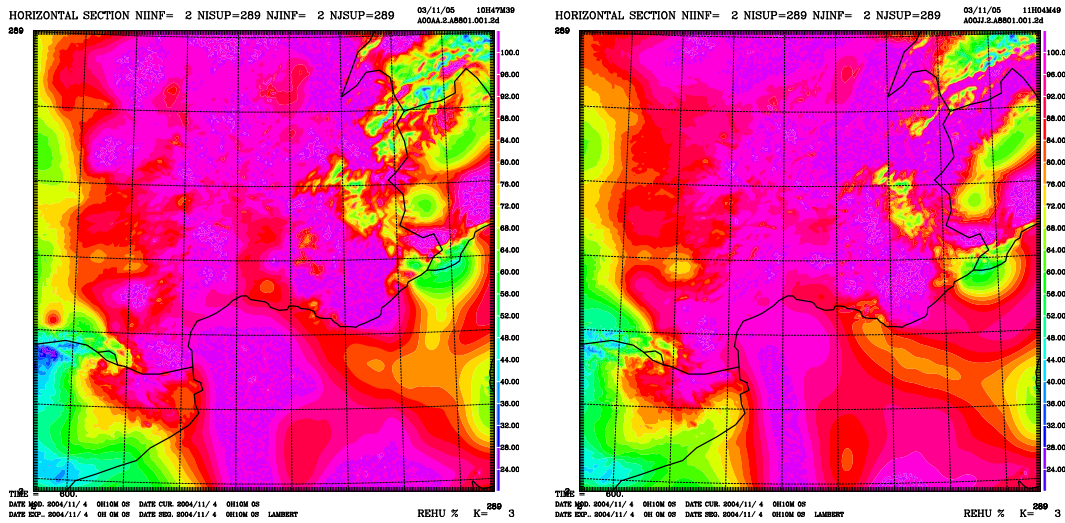
<sup>9</sup>It is used the same nomenclature present in Tab. 2



(a)  $J_B A$

(b)  $J_B B$

Figure 54: Potential temperature field at analysis time at 72 m a.g.l.



(a)  $J_B A$

(b)  $J_B B$

Figure 55: Humidity field at analysis time at 72 m a.g.l.

## C Test with assimilation of MSG/SEVIRI radiances

In the frame of a high-resolution assimilation for short-range forecasts, satellite radiances can recover the gap in vertical structure of atmosphere, and this results all the more important in an assimilation cycle with an hourly temporal step, when abundance of surface data can provide an accurate description of the boundary layer. Data from SEVIRI radiometer on board Meteosat-8 are used. So, a preliminary test has been conducted to evaluate the impact of radiances. Unfortunately, in the only test accomplished they do not appear to improve the forecasts. Model configuration is the same of Exp. AA. SEVIRI data assimilation is performed as in Aladin (Montmerle, 2004). Even if there are no anomalies in the first hour of forecasts, results show the overestimating tendency in 6-hours cumulated precipitation, in terms of both intensity and location of precipitating area.

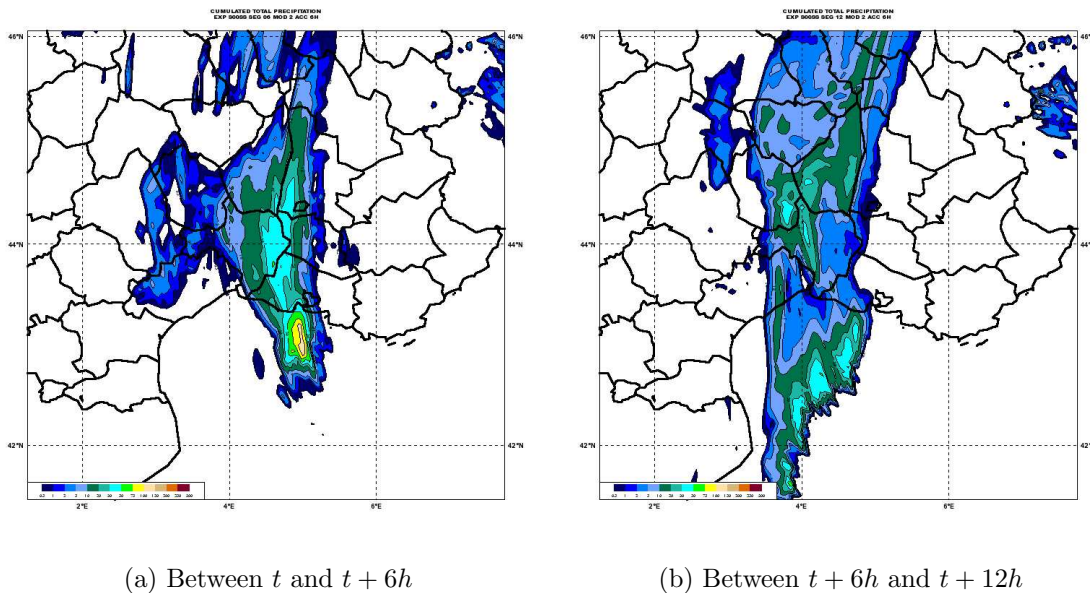


**Figure 56:** 6hr cumulated rain for Exp. SS

Briefly, evaluation of analyzed and forecasted fields let notice that the main feature of the Exp. SS for which forecasts overvalue rain's production is the increase in values of humidity. This is true in both low and middle atmosphere up to 4500 m over the western part of Languedoc-Roussillon region and mainly over sea. This is retrieved in the precipitation distribution.

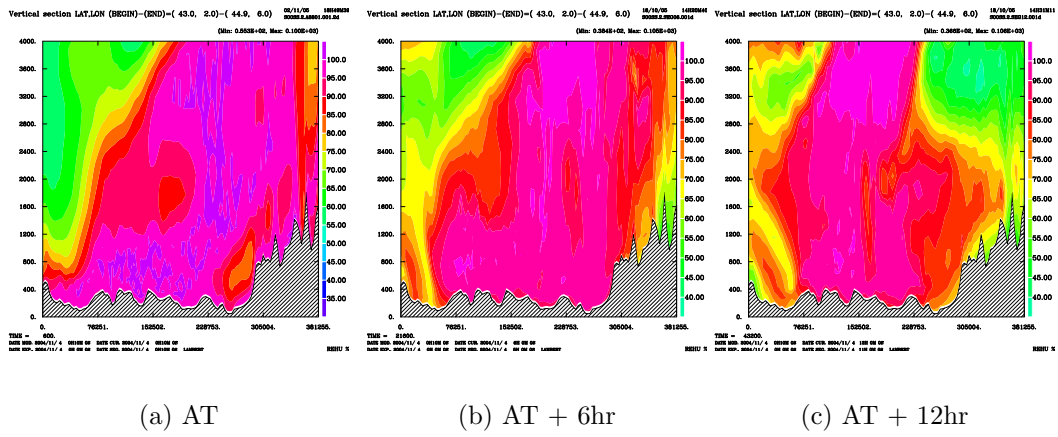


Figure 57: Exp. *SS* - Relative humidity in cross-section a-a'. Comparison has to be made with Fig. 16

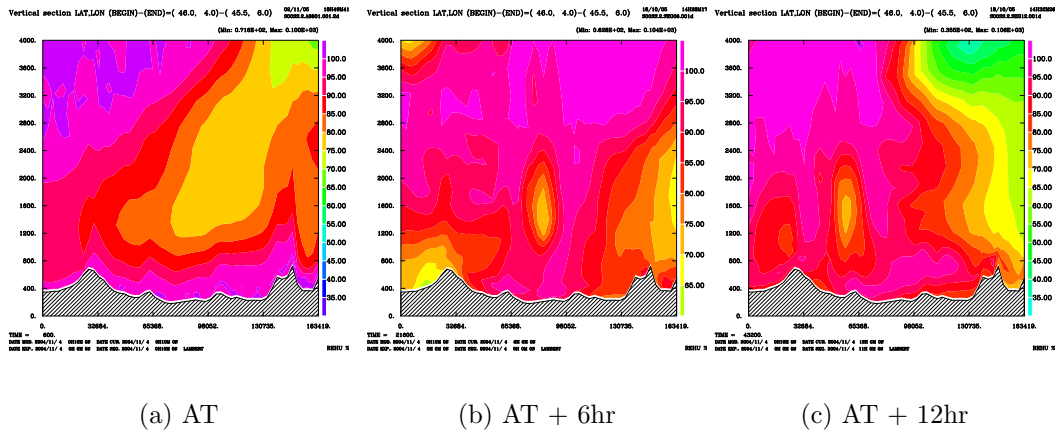
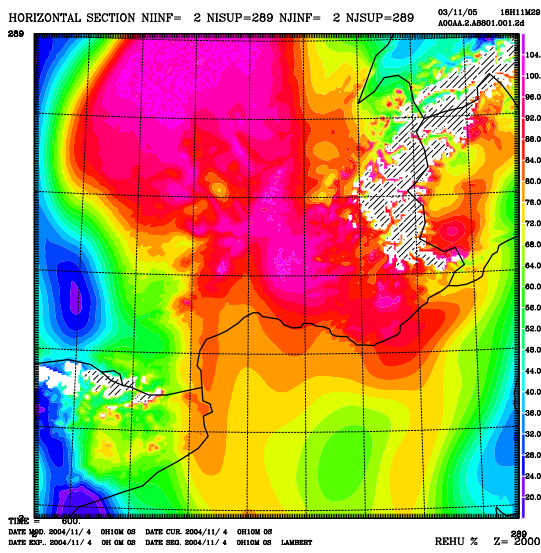
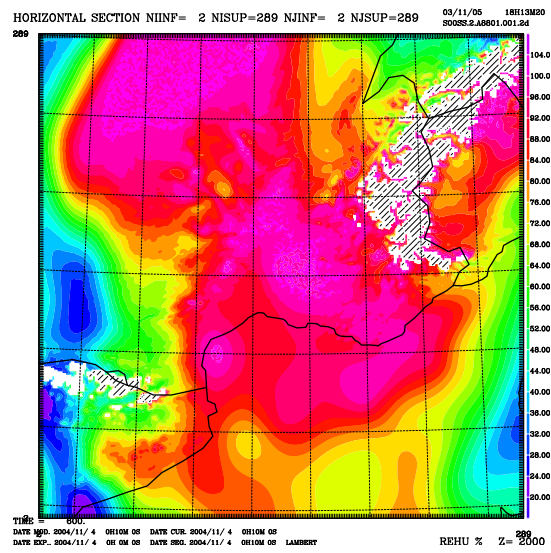


Figure 58: As Fig. 57 for cross-section b-b'. Comparison to has to be made with Fig. 18



(a) Exp. AA



(b) Exp. SS

Figure 59: Humidity at 2000 m

## References

- ACCADIA, C., S. MARIANI, M. CASAIOLI, A. LAVAGNINI, AND A. SPERANZA, 2003. Sensitivity of Precipitation Forecast Skill Scores to bilinear Interpolation and a Simple Nearest-Neighbour Average Method on High-Resolution Verification Grids. *Wea. Forecasting*, **18**, pp. 918–932.
- BALLARD, S., Z. LI, M. DIXON, S. SWARBRICK, O. STILLER, AND H. LEAN, 2005. Development of 1-4 Km resolution data assimilation for nowcasting at the Met Office. World Weather Research Program Symposium on nowcasting and very short range forecasting. WNO, Toulouse (France) 5-9 September 2005.
- BARKER, D. M., W. HUANG, Y. R. GUO, AND Q. N. XIAO, 2004. A Three-dimensional (3DVAR) data assimilation system for use with MM5: Implementation and initial results. *Mon. Wea. Rev.*, **132**, pp. 897–914.
- BELO PEREIRA, M. AND L. BERRE, 2005. The use of an Ensemble approach to study the Background Error Covariances in a Global NWP model. *Mon. Wea. Rev.* Accepted.
- BENGTSSON, L. AND K. I. HODGES, 2005. On the impact of humidity observations in numerical weather predictions. *Tellus A*, **57**, pp. 701–708.
- BOONE, A., J.-C. CALVET, AND J. NOILHAN, 1999. Inclusion of a third soil layer in a land-surface scheme using the force-restore method. *J. Appl. Meteor.*, **38**, pp. 1611–1630.
- BOUTTIER, F., 2003. The AROME mesoscale project. Seminar on recent developments in data assimilation for atmosphere and ocean. ECMWF, Reading (UK) 8-12 September 2003.
- CHERUBINI, T., A. GHELLI, AND F. LALAURETTE, 2002. Verification of precipitation forecasts over the Alpin region using a high-density observing network. *Wea. Forecasting*, **17**, pp. 238–249.
- CLARK, T. L., 1984. Severe downslope windstorm calculations in two and three spatial dimensions using anelastic interactive grid nesting: a possible mechanism for gustiness. *J. Atmos. Sci.*, **41**, pp. 329–350.
- CUXART, J., P. BOUGEAULT, AND J. L. REDELSPERGER, 2000. A turbulence scheme allowing for mesoscale and large-eddy simulations. *Q. J. R. Meteorol. Soc.*, **126**, pp. 1–30.

- DANCE, S. L., 2004. Issues in high resolution limited area data assimilation for quantitative precipitation forecasting. *Physica D*, **196**, pp. 1–27.
- DELRIEU, G. AND AL., 2005. The catastrophic flash-flood event of 8-9 September 2002 in the Gard region, France: a first case study for the Cévennes-Vivarais Mediterranean hydrometeorological observatory. *J. Hydrometeor.*, **6**, pp. 34–53.
- DUCROCQ, V., D. RICARD, J.-P. LAFORE, AND F. ORAIN, 2002. Storm-scale numerical rainfall prediction for five precipitating events over France: on the importance of the initial humidity field. *Wea. Forecasting*, **17**, pp. 1236–1256.
- EBERT, E. E., U. DAMRATH, W. WERGEN, AND M. E. BALDWIN, 2003. The WGNE assessment of short-term quantitative precipitation forecasts. *Bull. Amer. Met. Soc.*, **84**, pp. 481–492.
- FACCANI, C. AND R. FERRETTI, 2005. Data assimilation of high density observations: Part I. Impact on initial conditions for the MAP/SOP IOP2b. *Q. J. R. Meteorol. Soc.*, **131**, pp. 21–42.
- FACCANI, C., R. FERRETTI, AND G. VISCONTI, 2003. High resolution weather forecast over complex orography: sensitivity to the assimilation of conventional data. *Mon. Wea. Rev.*, **131**, pp. 136–154.
- FERRETTI, R. AND C. FACCANI, 2005. Data assimilation of high density observations: Part II. Impact on the forecast of the precipitation for the MAP/SOP IOP2b. *Q. J. R. Meteorol. Soc.*, **131**, pp. 43–62.
- GUSTAFSSON, N., P. LÖNNBERG, AND J. PAILLEUX, 1997. Data assimilation for high-resolution limited-area models. *J. Met. Soc. Jap.*, **75**, no. **1B**, pp. 367–382.
- HAMILL, T. M. AND J. JURAS, 2005. Common forecast verification metrics can overestimate skill. *Mon. Wea. Rev.* Submitted.
- JACQ, V., 1994. Inventaire des situations à précipitations diluviennes sur les régions Languedoc-Roussillon, Provence, Côte d’Azur et Corse, période 1958-1994. *Phénomènes remarquables*, **3**. Météo-France, SCEM, 190 pp.
- JAUBERT, G., P. BOUGEAULT, H. BERGER, B. CHIMANI, C. FLAMANT, C. HÖBERLI, M. LOTHON, M. NURET, AND S. VOGT, 2005. Numerical simulations of meso-gamma scale features of föhn at ground level in the Rhine valley. *Q. J. R. Meteorol. Soc.*, **131**, pp. 1339–1361.
- KAIN, J. S. AND J. M. FRITSCH, 1990. A one-dimensional entraining/detraining plume model and its application in convective parametrizations. *J. Atmos. Sci.*, **47**, pp. 2784–2802.

- LAFORE, J. P., J. STEIN, N. ASENSIO, P. BOUGEAULT, V. DUCROCQ, J. DURON, C. FISCHER, P. HEREIL, P. MASCART, J. P. PINTY, J. L. REDELSPERGER, E. RICHARD, AND J. VILA-GUERAU DE ARELLANO, 1998. The Meso-NH Atmospheric Simulation System. Part I: Adiabatic formulation and control simulations. *Annales Geophysicae*, **16**, pp. 90–109.
- MICHALAKES, J., S. CHEN, J. DUDHIA, L. HART, J. KLEMP, J. MIDDLECOFF, AND W. SKAMAROCK, 2001. Development of a next generation regional Weather Research and Forecasting Model. Proceedings of the 9<sup>th</sup> ECMWF Workshop on the use of high performance computing in meteorology. ECMWF, World Scientific, Singapore.
- MONTMERLE, T., 2004. Use of geostationary SEVIRI radiances in ALADIN 3D-VAR. Tech. rep., Aladin NWS Members. ALADIN Newsletter 27, July-December 2004.
- MORCRETTE, J.-J., 1989. Description of the radiation scheme in the ECMWF model. Tech. Rep. No 165, ECMWF.
- NURMI, P., 2003. Recommendations on the verification of local weather forecasts. Tech. Rep. No 430, ECMWF. 18 pp.
- PAILLEUX, J., 1997. Impact of observations in NWP models: summary of recent results and perspectives. Proceedings of CGC/WMO Workshop Impact of various observing systems on numerical weather prediction, pp. 193–198. WMO/TD, Geneve (Switzerland) 7-9 April 1997. No 868.
- PINTY, J.-P. AND P. JABOUILLE, 1999. A mixed-phase cloud parameterization for use in mesoscale non-hydrostatic model: simulations of a squall line and of orographic precipitations. Proceedings of Conference on Cloud Physics. Amer. Meteor. soc., Everett (WA, USA) August 1999.
- RADNÓTI, G., R. AJJAJI, R. BUBNOVÁ, M. CAIAN, AND E. CORDONEANU, 1995. The spectral limited-area model Arpège–Aladin. Tech. rep., WMO. PWPR report series n. 7 - WMO TD n. 699.
- ŠIROKA, M., C. FISCHER, V. CASSÉ, R. BROKOVA, AND J.-F. GELEYN, 2003. The definition of mesoscale selective forecast error covariances for a limited-area variational analysis. *Meteorol. Atmos. Phys.*, **82**, pp. 227–244.
- STEIN, J., E. RICHARD, J. P. LAFORE, J. P. PINTY, N. ASENSIO, AND S. COSMA, 2000. High-resolution non-hydrostatic simulations of flash-food episodes with grid-nesting and ice-phase parameterization. *Meteorol. Atmos. Phys.*, **72**, pp. 203–221.

- STEPPELER, J., G. DOMS, U. SCHÄTTLER, H. W. BITZER, A. GASSMANN, A. DAMRATH, AND G. GREGORIC, 2003. Meso-gamma scale forecasts using the nonhydrostatic model LM. *Meteorol. Atmos. Phys.*, **82**, pp. 75–96.
- THORNES, J. E. AND D. B. STEPHENSON, 2001. How to judge the quality and value of weather forecast products. *Meteorol. Appl.*, **8**, pp. 307–314.
- WWRP/WGNE, 2004. Recommendations for the verification and intercomparison of QPFs from operational NWP models. Tech. rep., WMO - WWRP/WGNE Joint Working Group on Verification.
- XIAO, Q. N., 2005. Assimilation of doppler radar observations using WRF/MM5 3D-Var system and his impact on short-range QPF. World Weather Research Program Symposium on nowcasting and very short range forecasting. WNO, Toulouse (France) 5-9 September 2005.

# Remerciements

Je tiens à remercier tout ces personnes qu'ont été, de façon consciente ou pas, un point de référence pendant les six mois au GMAP, particulièrement François pour m'avoir proposé ce stage, et Ludovic pour tout le temps qu'il a voulu me consacrer.